Observations of a Pc5 global (cavity/waveguide) mode outside the plasmasphere by THEMIS

Hartinger, Michael; Angelopoulos, Vassilis; Moldwin, Mark B.; Nishimura, Yukitoshi; Turner, Drew L.; Glassmeier, Karl-Heinz; Kivelson, Margaret G.; Matzka, Jürgen; Stolle, Claudia

Published in:
Journal of Geophysical Research

Link to article, DOI:
10.1029/2011JA017266

Publication date:
2012

Document Version
Publisher's PDF, also known as Version of record

Observations of a Pc5 global (cavity/waveguide) mode outside the plasmasphere by THEMIS

Michael Hartinger,[1] Vassilis Angelopoulos,[1] Mark B. Moldwin,[1,2] Yukitoshi Nishimura,[3,4] Drew L. Turner,[1] Karl-Heinz Glassmeier,[5] Margaret G. Kivelson,[1,2] Jürgen Matzka,[6] and Claudia Stolle[6]

Received 17 October 2011; revised 29 March 2012; accepted 23 April 2012; published 1 June 2012.

[1] Standing fast mode waves known as global modes, or cavity/waveguide modes, have been extensively studied as a potential driver of monochromatic shear Alfvén waves in the Earth's magnetosphere via the field line resonance (FLR) mechanism. However, their existence outside of the plasmasphere remains controversial. We present here a global mode observation outside the plasmasphere, using simultaneous multispacecraft observations in the solar wind, the magnetosheath and the outer magnetosphere, as well as ground magnetometer data. Broadband solar wind dynamic pressure fluctuations are the most likely drivers of the Pc5 frequency range (2–7 mHz) global mode. The global mode transfers energy toward the plasmapause, where it drives localized shear Alfvén wave activity in the Pc5 frequency range. Global modes are thus a viable mechanism for converting broadband energy sources to monochromatic, radially localized shear Alfvén waves in the Pc5 frequency range.

Citation: Hartinger, M., V. Angelopoulos, M. B. Moldwin, Y. Nishimura, D. L. Turner, K.-H. Glassmeier, M. G. Kivelson, J. Matzka, and C. Stolle (2012), Observations of a Pc5 global (cavity/waveguide) mode outside the plasmasphere by THEMIS, *J. Geophys. Res.*, *117*, A06202, doi:10.1029/2011JA017266.

1. Introduction

1.1. Monochromatic ULF Waves

[2] Ultra Low Frequency (ULF) waves are often observed on the ground in the Pc5 frequency range (~2–7 mHz) at mid to high latitudes. The wave activity is often monochromatic and in many cases localized in latitude [*Walker et al.*, 1979]. Sometimes the same frequency is observed at a wide range of latitudes [*Samson and Rostoker*, 1972]. Several mechanisms could provide a source of energy for these waves: wave-particle interactions with ring current ions [*Southwood et al.*, 1969], the drift-mirror instability [*Hasegawa*, 1969], magnetopause surface waves driven by the Kelvin-Helmholtz instability [*Southwood*, 1974; *Chen and Hasegawa*, 1974; *Fujita et al.*, 1996], quasi-monochromatic fluctuations in the solar wind [*Kepko et al.*, 2002], and global (or cavity/waveguide) modes [e.g., *Kivelson and Southwood*, 1985]. Observational evidence for the operation of the first four driver mechanisms exists; however, definitive evidence in the data for the operation of the global mode mechanism in the outer magnetosphere has been lacking, despite significant modeling efforts demonstrating its viability [e.g., *Allan et al.*, 1986a, 1986b; *Lee and Lysak*, 1989; *Claudepierre et al.*, 2009].

1.2. Global Mode Mechanism

[3] Global modes are standing fast mode waves trapped between different magnetospheric boundaries, such as the magnetopause, the plasmapause and/or the equatorial ionosphere [e.g., *Kivelson and Southwood*, 1986]. The global mode frequency is set by the transit time of fast mode waves, which in turn depends on the locations of the boundaries and the plasma environment within them. Global modes are expected to have perturbations in the east-west electric field and parallel magnetic field with a ~90 degree phase difference in time and nodal structure throughout their radial extent [*Waters et al.*, 2002].

[4] An example of the radial amplitude profile and phase for the compressional magnetic field perturbation associated with a cavity mode, a type of global mode, is shown in Figure 1, using the numerical model of *Zhu and Kivelson* [1989]. In this particular example, the Alfvén speed is assumed to vary monotonically as the inverse of the distance

[1]Earth and Space Sciences Department, University of California, Los Angeles, California, USA.
[2]Atmospheric, Oceanic, and Space Sciences Department, University of Michigan, Ann Arbor, Michigan, USA.
[3]Atmospheric and Oceanic Sciences Department, University of California, Los Angeles, California, USA.
[4]Solar-Terrestrial Environment Laboratory, Nagoya University, Toyokawa, Japan.
[5]Institute for Geophysics and Extraterrestrial Physics, Technical University of Braunschweig, Braunschweig, Germany.
[6]DTU Space, Technical University of Denmark, Copenhagen, Denmark.

Corresponding author: M. Hartinger, Earth and Space Sciences Department, University of California, 595 Charles E. Young Dr. E., Los Angeles, CA 90024, USA. (mhartinger@ucla.edu)

0148-0227/12/2011JA017266

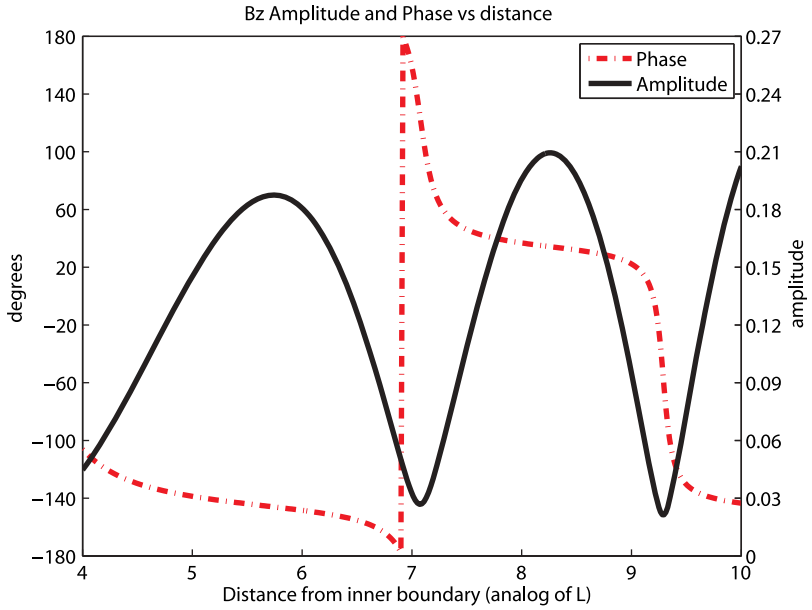

Figure 1. The model amplitude (black line) and phase (red dashed line) of the magnetic field perturbation along the background field as a function of radial distance, generated using the *Zhu and Kivelson* [1989] numerical model. In the model, the Alfvén speed varies as the inverse of the distance from the inner boundary; only one harmonic (eigenfrequency) is shown.

from the inner boundary. There are multiple nodes, or local amplitude minima, throughout the radial extent and there is a 180 degree rotation in phase of the perturbation on either side of each node, characteristic of global modes. The 360 degree jump seen at L $\sim$ 7 is not related to the spatial structure of the cavity mode; it occurs because the phase decreased below −180 degrees, causing it to wrap around to +180 degrees. Other numerical models have shown that significantly more structured global modes are possible and that non-monotonic Alfvén speed profiles and sharp density gradients play important roles in determining the behavior of global modes [e.g., *Zhu and Kivelson*, 1989; *Waters et al.*, 2002].

[5] The term global mode can refer to a number of different types of standing, fast mode waves, including cavity modes [*Kivelson and Southwood*, 1985] and waveguide modes [*Samson et al.*, 1992]. Both of these wave modes exhibit the features described above (e.g., nodal structure). The term cavity mode refers to a global mode in a closed magnetosphere; in other words, the only sink of energy is the ionosphere. The closely related waveguide mode has similar observational features to the cavity mode, but exhibits spatial and temporal dispersion as energy is allowed to leak into the magnetotail [*Wright*, 1994]. The differences between these two types of global modes are not important for the main results of this study.

[6] There are a number of potential drivers of global modes, including but perhaps not limited to dynamic pressure fluctuations [e.g., *Claudepierre et al.*, 2009], magnetosheath flows [*Mann et al.*, 1999; *Mills et al.*, 1999, 2000], fluctuations in the ion foreshock [e.g., *Takahashi et al.*, 2010], and Kruskal-Schwarzschild modes [*Plaschke et al.*, 2009]. *Wright and Rickard* [1995] showed that in the case of boundary motion with a broadband frequency spectrum, global modes can be excited when the frequencies for standing fast mode waves lie within the spectrum of the driver; *Claudepierre et al.* [2009] demonstrated that continual buffeting by broadband dynamic pressure fluctuations can effectively drive cavity modes in this manner. *Wright and Rickard* [1995] also showed that Alfvén waves can be excited if the standing fast mode frequencies lie within the range of accessible standing Alfvén wave frequencies in the magnetosphere cavity; in these cases, Alfvén waves will be excited at locations where the standing Alfvén wave frequency matches the global mode, or standing fast mode, frequency.

1.3. Alternative Mechanisms

[7] There are a few other sources of ULF waves with fluctuations parallel to the background magnetic field in the Pc5 frequency range. We note some of the properties of waves driven by these sources that are unique and can be used to differentiate them from global modes. Wave-particle interactions with ring current ions can generate ULF waves with antinodes (maximum amplitudes) in the radial magnetic field perturbation near the magnetic equator through a drift bounce resonance [*Southwood et al.*, 1969]. Waves driven by drift-bounce resonance are often associated with enhancements in hot (>1 keV) ions during the recovery phase of geomagnetic storms or during substorms [e.g., *Yang et al.*, 2010], which would cause an increase in the plasma β (ratio of thermal pressure to magnetic pressure). A spacecraft located where the wave is being driven ought to observe ion fluxes varying with the wave frequency at energies corresponding to drift and bounce frequencies that satisfy the resonance condition with the wave; furthermore, there should be a 180 degree phase difference between flux

variations observed above and below the resonant energy [*Southwood and Kivelson*, 1981].

[8] The drift-mirror instability is another mechanism for generating Pc5 ULF waves with parallel magnetic field perturbations. It occurs in high β plasmas and is associated with transverse magnetic field perturbations at the equator [*Cheng and Lin*, 1987]. Waves generated by the drift-mirror instability may also have compressional perturbations that are a harmonic of the transverse perturbations [*Hasegawa*, 1969; *Takahashi et al.*, 1990].

[9] There are also energy sources for ULF fluctuations in the Pc5 frequency range in the magnetosheath and solar wind, such as the Kelvin-Helmholtz instability (which drives magnetopause surface modes) or fluctuations in the solar wind dynamic pressure [e.g., *Fujita et al.*, 1996; *Kepko et al.*, 2002]. In the event that these sources of wave energy do not excite cavity or waveguide modes, they ought to directly drive parallel magnetic field perturbations that have amplitude monotonically decaying with increasing distance from the magnetopause, where the waves are being driven.

1.4. Previous Global Mode Observations and Observational Difficulties

[10] Substantial evidence has been presented for the existence of global modes in the plasmasphere, typically at frequencies above the Pc5 range [e.g., *Takahashi et al.*, 2010]. However, there have been few direct observations of global modes outside of the plasmasphere. *Kivelson et al.* [1997] reported observations of a compressional, quasi-monochromatic (24 mHz) perturbation of the magnetic field in the dayside magnetosphere, contrasted it to broadband fluctuations in the magnetosheath, and interpreted it as a cavity mode. *Mann et al.* [1998] used magnetic field data to identify compressional perturbations in the dawn and pre-noon sectors. Using two spacecraft and ground observations, they determined that significant spatial and temporal dispersion occurred, consistent with a waveguide mode. *Rickard and Wright* [1995] proposed that few cavity modes have been observed because dispersion, expected for regions that are better described as cavities than waveguides, would preclude the observation of a monochromatic signal. One would then expect broadband observations similar to *Mann et al.* [1998] rather than monochromatic observations similar to *Kivelson et al.* [1997]. Finally, *Eriksson et al.* [2006] identified perturbations on the dayside as being associated with a tailward propagating waveguide mode that was strongly coupled to locally standing Alfvén waves.

[11] *Kivelson et al.* [1997] noted several possible reasons why so few cavity modes have been observed; these reasons apply to other global modes:

[12] 1) The quality factor of the magnetospheric resonator is low and cavity modes damp quickly.

[13] 2) The energy sources (drivers) for cavity modes are rarely steady for long enough for a spacecraft to identify the global structure of the cavity mode.

[14] 3) To sustain a cavity mode, the cavity must be stable in size and configuration. This means that, for example, there cannot be large changes in the solar wind dynamic pressure that significantly change the location of the magnetopause on a timescale similar to or less than one wave period. Additionally, the geomagnetic activity should be low, since processes internal to the Earth's magnetosphere can also alter its configuration.

[15] 4) Amplitudes of compressional fluctuations associated with fast mode waves are small because the wave energy can rapidly spread out in all directions, unlike Alfvén wave modes. This suggests that other sources of ULF wave activity could often obscure cavity modes and that they might often be below the detection threshold of electric and magnetic field instruments.

[16] 5) A spacecraft must be located close to the magnetic equator to identify a cavity mode, since that is where most of the wave energy is confined [*Zhu and Kivelson*, 1991]. It must also be moving radially, or be in a radial alignment with other spacecraft, to identify the global structure of the cavity mode.

1.5. Overview of Study

[17] The above list provides guidelines for finding intervals that are ideal for determining whether ULF wave activity is consistent with the presence of global modes. Such intervals should occur when:

[18] 1) A particular driver of ULF waves provides a continual source of energy over several wave cycles.

[19] 2) There are no large fluctuations in solar wind dynamic pressure or other phenomena that could cause a rapid (timescale less than a few wave periods) change in the size of the magnetosphere.

[20] 3) Geomagnetic activity is low and there are no other major sources of ULF wave activity.

[21] 4) Several radially separated observations are available near the magnetic equator.

[22] We used these guidelines to identify intervals where conditions were ideal for global mode identification. To find such intervals, we required periods when multipoint observations are available in the magnetosphere near the magnetic equator, in the magnetosheath, and in the solar wind. Once such intervals were identified, we used the electric and magnetic field data from probes in the magnetosphere to identify intervals where the wave polarization was consistent with global modes and inconsistent with other wave modes.

[23] The purpose of this paper is to identify global mode oscillations during one such interval in the dawn sector in the region outside of the plasmasphere on 13 Nov 2008. Using observations in the solar wind, magnetosheath, magnetosphere, and on the ground, we determine that broadband dynamic pressure fluctuations in the solar wind are converted into a monochromatic global mode with Pc5 frequency (6.5 mHz). We also observe energy flux directed earthward from the location of the global mode observation and toward the plasmapause; at the plasmapause, we find that standing Alfvén wave activity is occurring in the same frequency range as the global mode.

[24] We present our results in the next five sections. In section 2 of this paper, we describe the instrumentation used in this study. In section 3, we provide an overview of the event and the criteria we used to select a short interval when the global mode is observed. In section 4, we describe wave polarization, energy transfer, time evolution, spatial structure, and the relationship between electron density and wave activity during this shorter interval. In section 5, we describe how these wave properties are inconsistent with several mechanisms that have previously been shown to drive waves

in the Pc5 frequency range. In section 6, we describe how the wave properties are consistent with the global mode mechanism and further characterize the global mode. Finally, we summarize our results in section 7.

2. Instrumentation

[25] For magnetosphere, magnetosheath, and solar wind observations we use data from the five-satellite Time History of Events and Macroscale Interactions (THEMIS) spacecraft [*Sibeck and Angelopoulos*, 2008]. Each spinning satellite (3 s spin period) is equipped with a fluxgate magnetometer (FGM) [*Auster et al.*, 2008], an electric field instrument (EFI) [*Bonnell et al.*, 2008], an ion and electron electrostatic analyzer (ESA) [*McFadden et al.*, 2008a], and ion and electron solid state telescopes (SST) [e.g., *Ni et al.*, 2011].

[26] EFI measures ULF fluctuations best in the spin plane of the spacecraft; we obtain the component along the spin axis using the $\vec{E} \bullet \vec{B} = 0$ approximation when the normal of the spin plane is at a large angle to the background magnetic field direction; in this study, the angle was always larger than 20 degrees. The measurement of the amplitude and phase of ULF waves by EFI is affected by several sources of contamination. In Appendix A and the auxiliary material, we describe these sources of contamination, how they can be routinely identified and removed, and how we determined which THEMIS EFI data were useable for the present study.[1] ESA measures the three-dimensional particle distributions and moments (electrons: 5 eV–30 keV, ions 5 eV–25 keV) once per spin. SST also measures the three-dimensional particle distributions and moments once per spin and is sensitive to energies above 25 keV; however, calibration of the SST instrument is ongoing and the highest quality data for this study is only available at ∼5 min resolution. We obtained all THEMIS data directly from the THEMIS website (http://themis.ssl.berkeley.edu/index.shtml) and applied the latest calibrations and corrections using the software package distributed by the THEMIS science team. For ground magnetometer observations, we use 1 s data from Greenland magnetometers from DTU Space at the Technical University of Denmark.

3. Event Overview and Selection

3.1. Overview of Geomagnetic Activity and Solar Wind Conditions

[27] The global mode event occurred on 13 Nov 2008 during a prolonged period of low geomagnetic activity. Solar wind data and geomagnetic activity indices (obtained from the NASA Space Science Data Facility through OMNIweb - http://omniweb.gsfc.nasa.gov/) for several days leading up to the event are shown in Figure 2, with the interval of interest highlighted in pink. The *Kp*, *Dst*, and *AE* indices all indicate quiet geomagnetic activity levels (first, second, and third panels in Figure 2). The event occurred during an interval of solar wind flow speed of ∼310 km/s (fifth panel in Figure 2) and typical number density of ∼6 protons per cubic centimeter (fourth panel in Figure 2).

3.2. Solar Wind and Magnetosheath Data During the Event

[28] More detailed, higher time resolution information from the solar wind and magnetosheath are given in Figure 3. Figure 3a shows the positions of the THEMIS probes in the GSM xy plane, along with the statistical location of the magnetopause and bow shock derived from the *Shue et al.* [1997] and *Fairfield* [1971] models, respectively. Selected solar wind, magnetosheath, and ground magnetometer observations are shown in Figure 3b from THEMIS-B (THB), THEMIS-C (THC), and the Tasiilaq (code AMK, former name Ammassalik) and Nuuk (code GHB, former name Godthaab) ground magnetometers for the period from 0600 to 0820 UT. AMK is located at 65.60° geographic north and 322.37° east and GHB is located at 64.17° geographic north and 308.27° east. We used field line tracing software from the French National Aerospace Research Center (ONERA) with the *Tsyganenko* [1989] model to determine that AMK mapped to THEMIS-D's (THD) location during the period from 0600 to 0820 UT, whereas GHB mapped to a location ∼1.5 Earth radii (Re) further away from the Earth and ∼3 Re tailward of AMK's location. The *Tsyganenko* [1989] model predicted the magnetic field magnitude to within 9% and the magnetic field direction to within 9° at 0700 UT at all THEMIS probes in the magnetosphere, suggesting that it is suitable for mapping the magnetometers' locations.

[29] The first panel in Figure 3b shows the solar wind ion energy flux spectrogram. Reflected ions with energies ≥1 keV ions are seen at the beginning of the interval, when the ion foreshock is located in the dawn sector. After 0625 UT, the interplanetary magnetic field (third panel in Figure 3b) reorients, the ion foreshock moves away from the dawn sector, and THB measures the pristine solar wind. The IMF GSM z component is primarily positive until 0745 UT, the solar wind velocity is ∼310 km/s (second panel in Figure 3b), and small dynamic pressure fluctuations are seen with a maximum amplitude of about 0.15 nPa (fourth panel in Figure 3b). The lower than nominal solar wind speed and the steady, positive IMF *z* component suggest that neither flux transfer events (FTEs) nor magnetopause surface waves driven by the Kelvin-Helmholtz instability will be present between 0625 and 0745 UT. The absence of these features is confirmed by THEMIS-C (THC), which is located in the magnetosheath; in the fifth panel in Figure 3b an ion energy flux spectrogram shows no significant transient features or surface wave activity. The IMF begins to turn southward at 0735 UT and turns sharply southward at 0745 UT (third panel in Figure 3b); these changes likely caused a flux transfer event that THC observes at 0800 UT (fifth panel in Figure 3b). This southward turning could have produced a change in the magnetopause location [*Shue et al.*, 1997] as well as transient ULF wave activity in the magnetosphere before 0800 UT, as THC is located close to the dawn flank and there is a time delay between the initial interaction at the bow shock nose and the arrival of the flux transfer events or other changes at THC's location.

3.3. ULF Wave Drivers

[30] We used ground based observations from AMK and GHB for initial examination of the ULF wave activity and its

[1] Auxiliary materials are available in the HTML. doi:10.1029/2011JA017266.

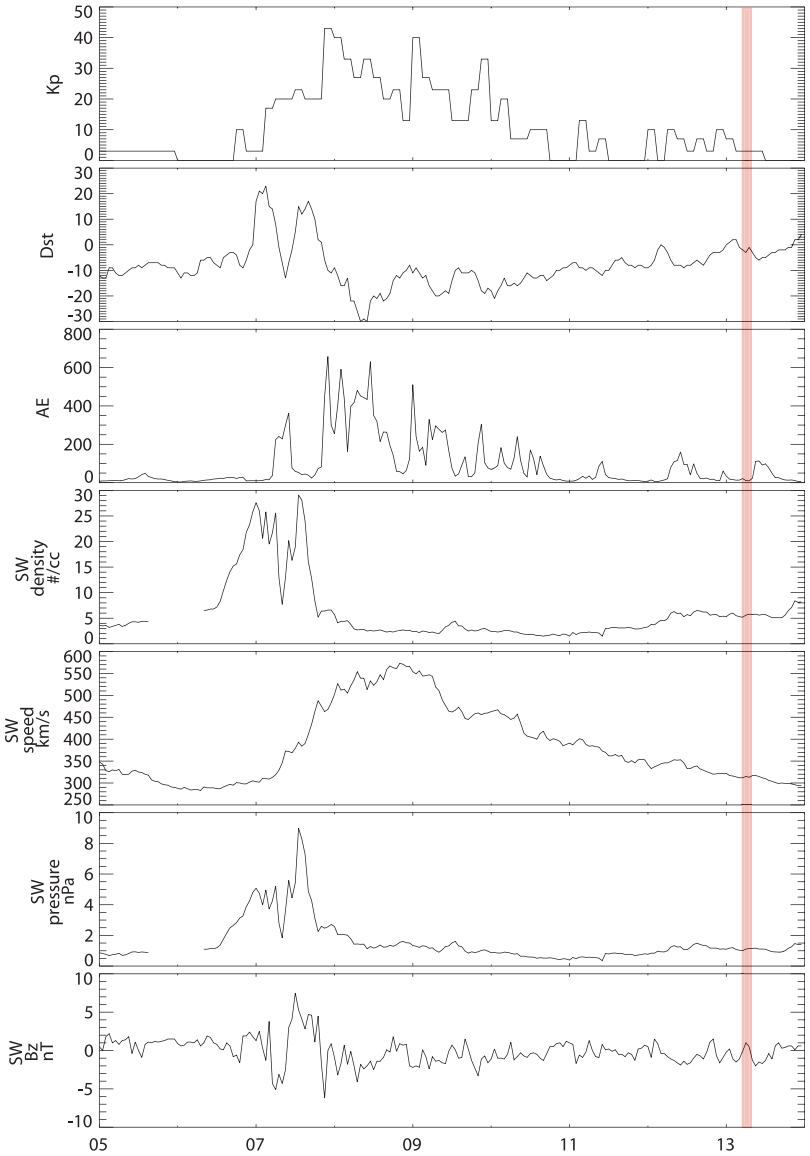

Figure 2. From top to bottom, *Kp**10, *Dst*, *AE*, solar wind density, solar wind speed, solar wind pressure, and the GSM z component of the interplanetary magnetic field, obtained from OMNIweb (http://omniweb.gsfc.nasa.gov/). The shaded pink region indicates the interval of interest for this study.

relationship with conditions in the solar wind and magnetosheath. Unlike spacecraft moving near the magnetic equator, ground magnetometers such as AMK map to positions near the magnetic equator that change little over time (their mapped position changes slightly due to stretching on the nightside and compression on the dayside). The power in magnetic fluctuations at a ground station can be interpreted without concern for the ambiguity that would arise, for example, in interpreting spacecraft data that could not distinguish between a global increase in wave power and a local increase arising from approach to an antinode of a standing wave. Thus, for the present study, ground based observations are more useful for examining temporal changes in ULF wave activity and their relationship with time variable driving conditions than in situ observations.

[31] ULF wave activity is seen on the ground in the high-pass filtered (frequency >0.5 mHz) H component at AMK (sixth panel in Figure 3b). We shifted the solar wind dynamic pressure data from THB by 310 s, accounting for the solar wind propagation time from the bow shock nose to THB's downstream location, to study the response of the magnetosphere to solar wind fluctuations at the bow shock nose. We then applied a running, 512 point (26 min) Fast Fourier Transform (FFT) to the solar wind dynamic pressure and ground magnetometer H component quantities at AMK and GHB during the interval when the IMF was predominately northward (indicated by the red lines in Figure 3b). For each FFT window, we computed the average power spectral density (PSD) in the range from 1 to 50 mHz.

[32] We normalized the PSD from AMK and GHB to the maximum value observed at each magnetometer in order to show the time evolution of the PSD rather than differences in the absolute value of the PSD between the two stations. We used the 1 to 50 mHz frequency range for two reasons.

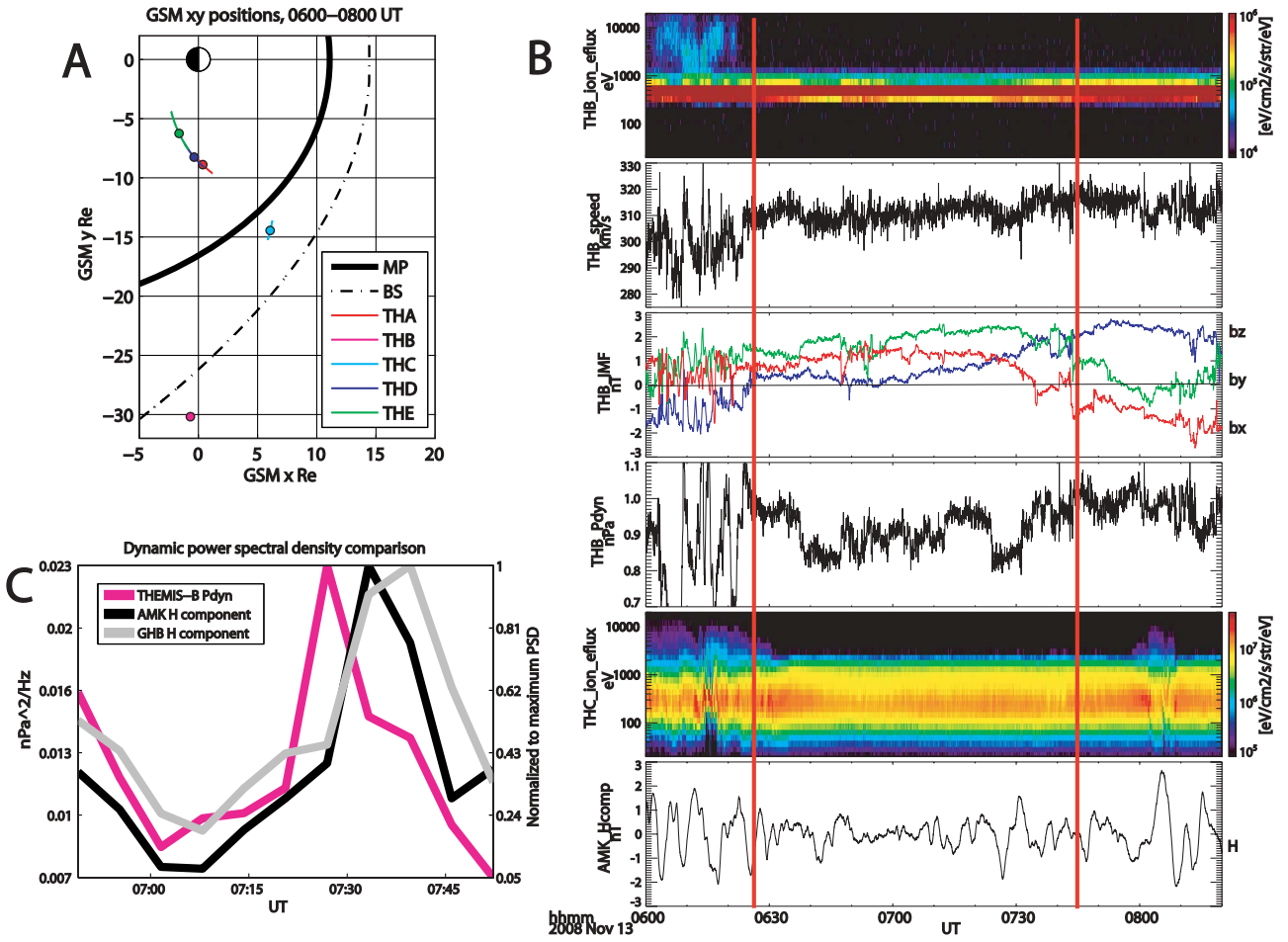

Figure 3. (a) The GSM xy plane showing the orbits of 5 THEMIS probes from 0600 to 0800 UT (lines) and their position at 0700 UT (dots), with the location of the magnetopause as a solid black line and the location of the bow shock as a dot-dashed line. (b) From top to bottom, (1) ion energy flux spectrogram from THB, (2) plasma speed at THB calculated using ESA electrons, (3) the GSM components of the magnetic field at THB, (4) the dynamic pressure at THB calculated using ESA electrons, (5) the ion energy flux spectrogram from THC, (6) the H component of the high pass filtered (>0.5 mHz) magnetic field at the Tasiilaq (AMK) ground magnetometer, which maps to a region very close to THD. (c) The power spectral density averaged over the 1 to 50 mHz frequency band during the interval from 0630 to 0800 UT (marked by red lines in Figure 3b) for dynamic pressure fluctuations (pink) and ground magnetic field fluctuations at AMK (black) and Godthaab (GHB); GHB maps to a region ~1.5 Re outside and ~3 Re tailward of THD's location.

One was to facilitate comparisons of the time evolution of wave power between the two stations. The local resonant field line frequency is different at the two stations, and examination of the time evolution of wave power would be difficult if a narrower frequency range was chosen that overlapped with the fundamental or harmonics of standing Alfvén waves at one station and not the other. We are interested in the global dependence of ULF wave activity on solar wind dynamic pressure fluctuations, so we chose a larger frequency range to remove these regional differences. Another reason we chose the 1 to 50 mHz frequency range was to examine whether dynamic pressure fluctuations are an important source of energy for ULF waves over a large frequency range. It is possible for different mechanisms to drive ULF waves at different frequencies. However, if the magnetic field perturbations observed at ground stations are correlated with dynamic pressure fluctuations in the solar wind over a broad frequency range, it suggests that dynamic pressure fluctuations are the most important energy source for ULF waves.

[33] The running averages for all three quantities are shown in Figure 3c. ULF wave power variations at two different stations on the ground appear to follow well the ULF wave power in the solar wind dynamic pressure. Since the ground stations map to locations near the THEMIS probes in the magnetosphere, we conclude that broad band solar wind dynamic pressure fluctuations are the main driver of ULF wave activity in the region near these THEMIS

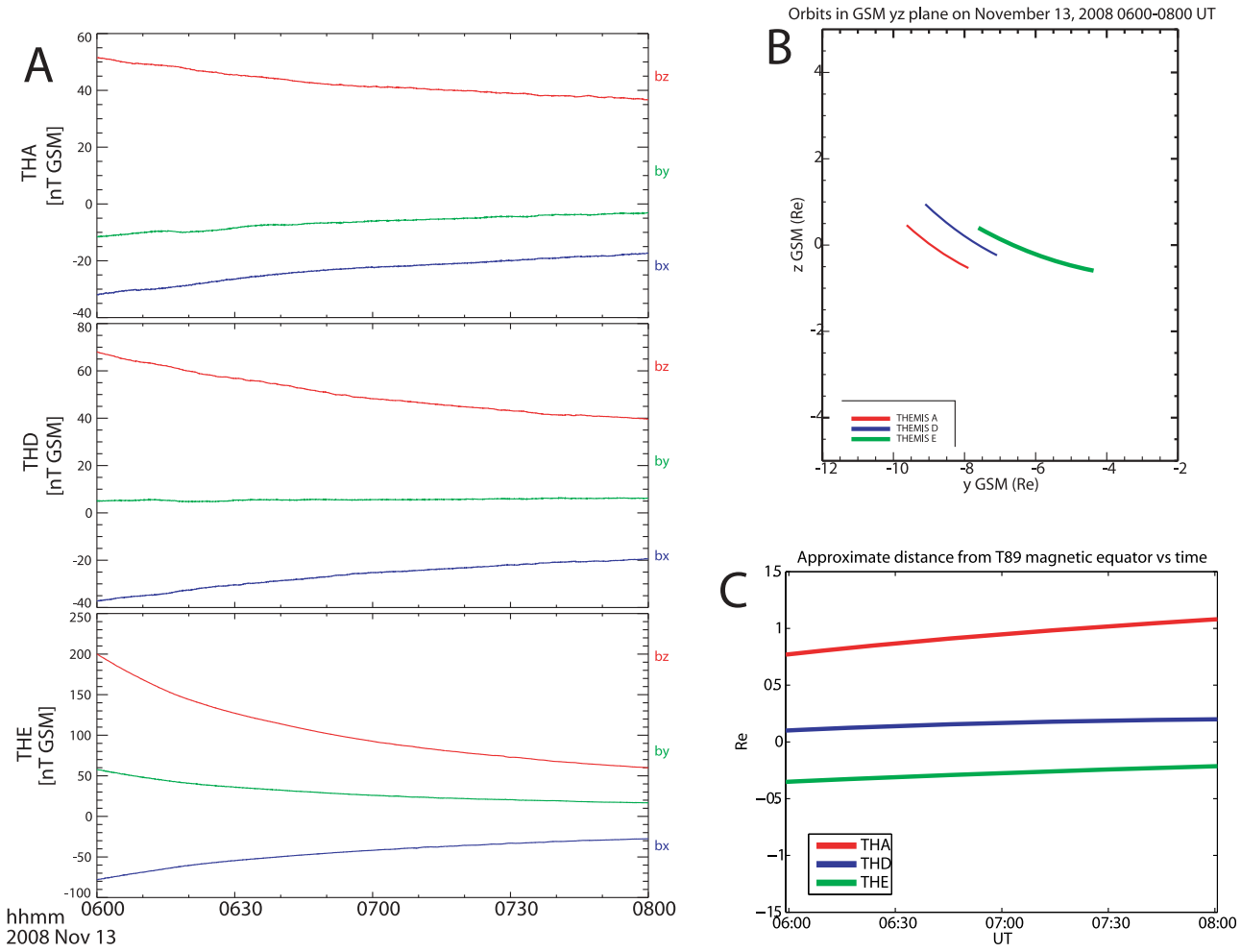

Figure 4. (a) From top to bottom, magnetometer data from THA, THD, and THE in GSM coordinates. In each panel, red is for the GSM *z* component, green is for the GSM *y* component, and blue is for the GSM *x* component. If a probe is near the magnetic equator and on the dawn meridian, the GSM y component of the magnetic field ought to be small compared to the other components. (b) The orbits of THA (red), THD (blue), and THE (green) from 0600 to 0800 UT projected onto the GSM *yz* plane. (c) The approximate distance from the geomagnetic equator, as computed with the *Tsyganenko* [1989] model, for THA (red), THD (blue) and THE (green).

probes after the ion foreshock moved away from the dawn sector but before the IMF turned sharply southward (~0625 to 0745 UT).

3.4. Location of Probes Relative to Magnetic Equator

[34] THEMIS-A (THA), THEMIS-D (THD), and THEMIS-E (THE) are located in the magnetosphere in the dawn sector during this interval (Figure 3a). All probes were very close to the magnetic equator where fast mode wave energy is expected to be confined, as shown in Figure 4 [*Zhu and Kivelson*, 1991]. We used two methods to determine the location relative to the magnetic equator: inspection of magnetometer observations and magnetic field models of the location of the magnetic equator. In Figure 4a, we show magnetometer data from each THEMIS probe in GSM coordinates. Near the dawn meridian, the GSM *y* component ought to be small compared to the other components if a probe is near the magnetic equator, and this is indeed the case. In Figure 4b, we show the probe locations in the GSM *yz* plane, confirming that they are close to the geomagnetic equator (since the GSM *z* coordinate is small for all probes). To account for the fact that the position of the magnetic equator in a distorted magnetic field may differ from the position of the dipole magnetic equator to varying degrees at different magnetic local times, we used the ONERA software package to determine the location of the magnetic equator as a function of time using the *Tsyganenko* [1989] magnetic field model, which we have already validated as a reliable model for this interval (when mapping AMK to THD's location – see section 3.2). The software determines the location of the magnetic equator by tracing along a field line from each satellite's position to the magnetic equator at each instant in time. In Figure 4c, we plot the approximate distance from the geomagnetic equator using the GSM *z* separation between each probe's position and the magnetic equator position as a function of time. All probes are within ~1 Re of

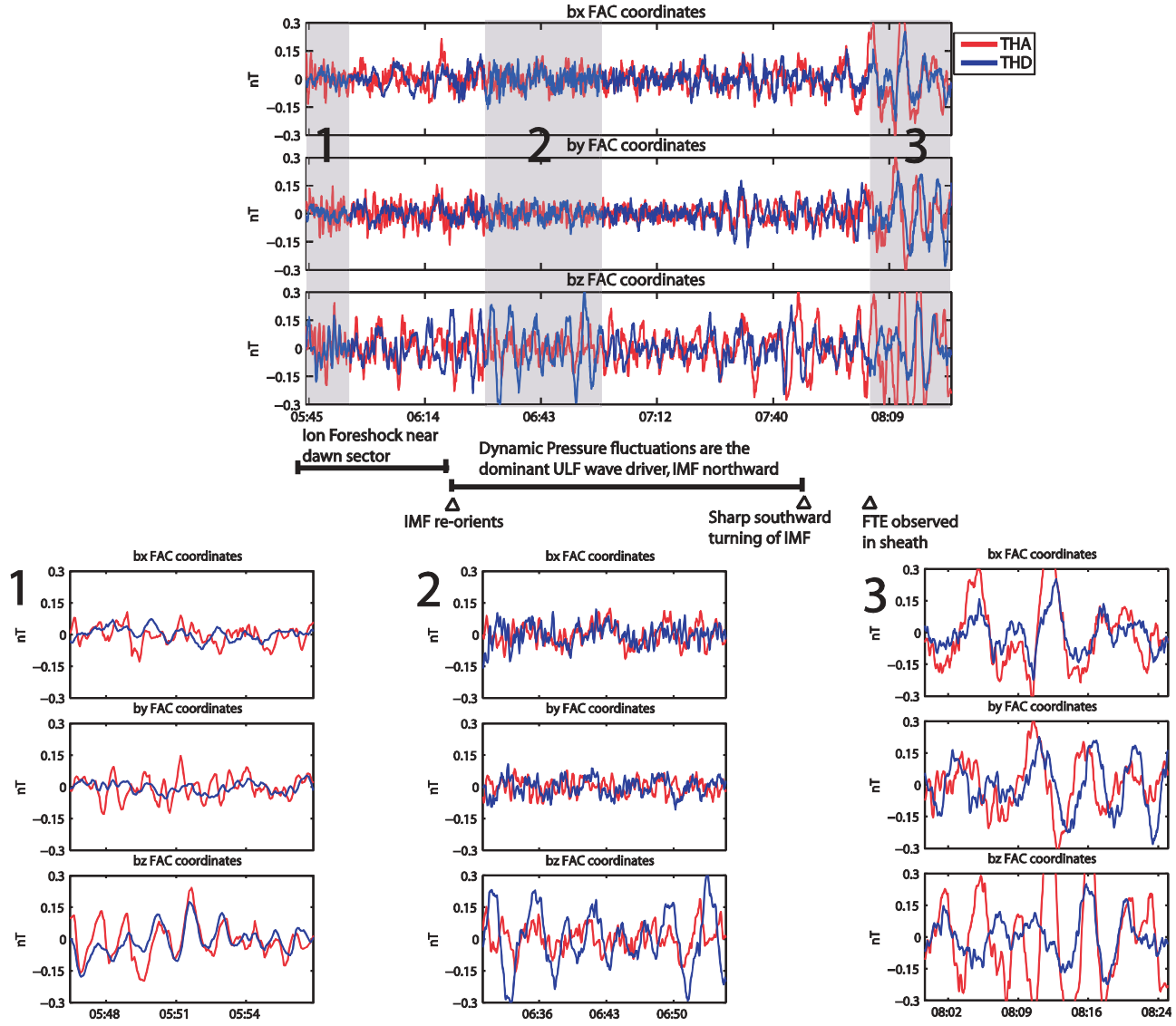

Figure 5. (top) Traces for each field-aligned coordinate (FAC) component are shown for THA (red) and THD (blue). The z component is on the top, y in the middle, and x on the bottom. The solid black lines indicate the interval of interest for this study. (bottom) Corresponding traces for the three numbered, gray shaded areas in Figure 5 (top), displayed in the same manner. They show the same data as in Figure 5 (top) but for smaller time intervals.

the geomagnetic equator during this interval, or have geomagnetic latitudes of less than ~3 degrees.

3.5. Overview of ULF Wave Activity Observed In Situ

[35] The probes in the region of primary interest are THA and THD. ULF wave activity observed by THA and THD from 0545 to 0825 UT is shown in Figure 5 (top), with smaller time intervals in Figure 5 (bottom). For analysis of the wave data, we use a field-aligned coordinate (FAC) system in which z is along the background magnetic field, y points eastward, and x completes the right-hand orthogonal set pointing radially outward. From top to bottom, the high pass filtered (frequency >2 mHz) magnetic field x, y, and z components are shown; red is for THA, blue is for THD. Throughout much of the interval, the z component perturbations are larger than those for the x and y components for both probes, indicating that compressional waves dominate.

[36] Since THA and THD are separated by less than one Earth radius during this interval, propagating fast mode waves originating from a source remote from this region (e.g., the magnetopause) ought to arrive at nearly the same time, since the transit time is comparable to the magnetic field sampling rate. Inspection of a shorter time interval from 0547 to 0557 UT in Figure 5 (bottom left) shows that this is indeed the case; compressional waves with ~1 min period are seen by both probes with similar amplitude and with no phase difference evident. The ion foreshock was located in the dawn local time sector during this interval and was likely the dominant source of wave activity in this region of the magnetosphere (see Figure 3).

[37] A later time interval is shown in Figure 5 (bottom middle), during a period when the ion foreshock is no longer present in the dawn sector and dynamic pressure fluctuations

are the main source of wave activity. As in Figure 5 (bottom left), compressional perturbations dominate. However, the wave period is 3 times larger than before (~3 min) and is only noticeable at THD (blue), despite the fact that THD is further from the magnetopause than THA. Finally, in Figure 5 (bottom right) we examine an interval after the IMF turned southward and at about the same time that THC observed a flux transfer event in the magnetosheath in the dawn sector; compressional perturbations no longer dominate, the perturbations of all components are generally larger than before, and the z perturbations have longer period than before (~4–5 min) and are more irregular.

3.6. Summary of Event Overview and Selection

[38] To summarize, we have identified an interval where the geomagnetic activity was low and several probes were in a favorable radial alignment near the geomagnetic equator in the dawn sector of the magnetosphere. Using one probe in the solar wind, one in the magnetosheath, and two ground magnetometers we determined that dynamic pressure fluctuations were the dominant driver of ULF wave activity in the dawn sector magnetosphere and the IMF was steady and primarily northward from ~0625 to ~0745 UT with no large changes in the overall dynamic pressure. Finally, using two probes separated by less than 1 Re in the magnetosphere, we drew several distinctions between ULF wave activity observed before 0625 UT, from 0625 to 0745 UT, and after 0745 UT.

[39] We conclude that the interval from 0625 to 0745 UT is ideal for investigating whether the fluctuations observed are consistent with the presence of a global mode, as there is one dominant driver of ULF waves (dynamic pressure) with no significant transient sources of wave activity, the size of the magnetospheric cavity is expected to be stable as the IMF GSM z component is positive and there are no large changes in dynamic pressure [*Shue et al.*, 1997], and there is a favorable alignment of several probes near the geomagnetic equator. These criteria are consistent with the guidelines motivated by *Kivelson et al.* [1997] that were described in section 1. We next turn our attention to the wave activity during this shorter interval.

4. ULF Wave Properties

4.1. Multispacecraft Power Spectral Density Comparisons

[40] From top to bottom in Figure 6, the dynamic power spectrum for the x, y, and z components (FAC system) of the high pass filtered magnetic field (frequency >2 mHz) are shown for THA (first, second, and third panels in Figure 6) and THD (fourth, fifth, and sixth panels in Figure 6) for the same interval as in Figure 3b, with the frequency range extending from 2 to 11 mHz in each panel. We also show a dynamic power spectrum for the solar wind dynamic pressure measured at THB in the seventh panel of Figure 6, where we have whited out time intervals when THB is located in the ion foreshock and not in the pristine solar wind (and thus cannot directly measure the solar wind dynamic pressure). We used a 1024 point (~50 min) FFT window, applied a Hanning window before computing the power spectrum, and smoothed the data in the frequency domain to reduce noise.

[41] For much of the interval shown in Figure 6, compressional magnetic field perturbations (z component) are dominant at both probes. There is enhanced wave power at several frequencies. For example, in the third panel in Figure 6 at 0700 UT, there are perturbations at 6.5 mHz and 4 mHz observed by THA. These frequencies are also evident at THD during the interval between the black lines. We focus on the 6.5 mHz power enhancements by demarcating the 5.5 to 8 mHz frequency band with black arrows on the frequency axis in each panel. For the entire interval, there are perturbations only in the z, and to a lesser extent x, components in this frequency band. Enhancements in power at 6.5 mHz do not occur at the same time at both probes suggesting that the probes are moving through a spatial structure.

[42] The dynamic power spectrum for the solar wind dynamic pressure shows enhanced wave power at a broader band of frequencies than observed at the THEMIS probes. Notably, the strongest enhancements in power in the 6.5 mHz frequency band (e.g., at 0730 UT) do not coincide with enhancements in power at the THEMIS probes. If broadband dynamic pressure fluctuations are the source of energy for the 6.5 mHz fluctuations at the THEMIS probes, as is suggested by the correlation between broadband dynamic pressure fluctuations and ULF wave power observed on the ground (Figure 3c), this suggests that the amplitude of the ULF waves is changing primarily due to passage through spatial structures rather than the temporal variation of the driver. Such a scenario was proposed by *Wright and Rickard* [1995]; they demonstrated that a driver with a broadband frequency spectrum could excite global modes with discrete frequencies. These global modes can act as reservoirs of energy, storing energy from the driver and exhibiting persistent spatial structure even if the energy supplied by the driver varies in time.

4.2. Wave Polarization

[43] For the remainder of section 4, we will focus on the 6.5 mHz signal, because observations shown in Figure 6 suggest that it exhibits spatial structure as expected for a global mode. We examine both the electric and magnetic field data from THD during the interval marked by the black lines in Figure 6. This interval is best suited to examining the wave polarization properties because both the electric and magnetic field perturbations are finite and measurable in the 6.5 mHz frequency band and are distinguishable from other frequencies. We use THD because electric field measurements on THA are contaminated throughout its entire outbound trajectory (see Appendix A and auxiliary material).

[44] The high pass filtered (frequency >0.5 mHz) magnetic field z and electric field y components, respectively, are shown in Figure 7 as black traces. A ~3 min period (~6.5 mHz) signal is seen between 0635 and 0650 UT, with an amplitude of ~100 pT in the magnetic field and ~0.8 mV/m in the electric field. Overplotting the band-pass filtered (5 to 8 mHz) signal in the first and second panels in Figure 7 (red traces) shows that the raw ~6.5 mHz signal phase has not been altered by our processing. In the third panel in Figure 7, the band pass filtered electric field y component (red) and magnetic field z component (blue) are overplotted. In the fourth panel in Figure 7, we use a Hilbert transform technique adapted from *Glassmeier* [1980] to compute the cross phase; a phase difference close to 90° is

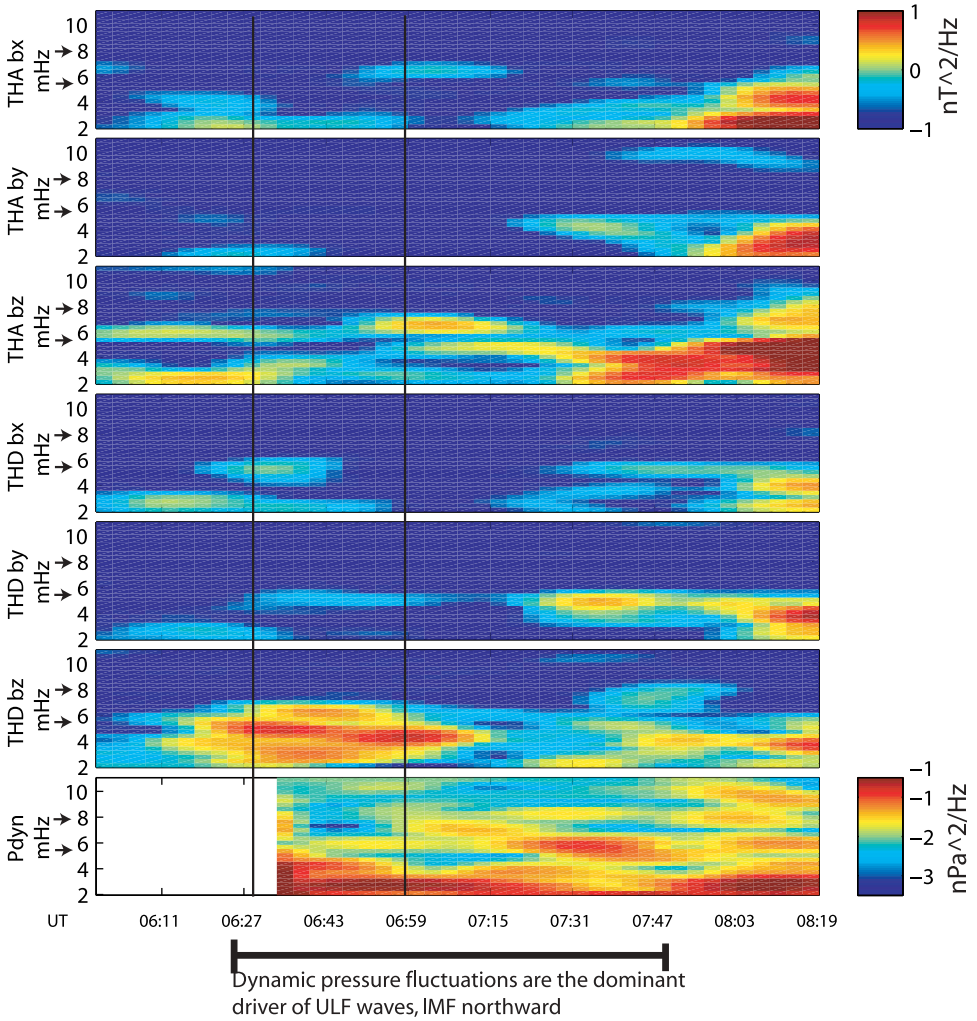

Figure 6. From top to bottom, the dynamic power spectrum for the *x*, *y*, and *z* components (field-aligned coordinates) for THA magnetic field data, the *x*, *y*, and *z* components for THD magnetic field data, and for the solar wind dynamic pressure fluctuations measured at THB. The solid black lines indicate the interval shown in Figure 7. The black arrows on the frequency axes demarcate the 5.5 to 8 mHz frequency band.

seen in the third and fourth panels in Figure 7, as expected for a global mode.

[45] The electric field *x*, magnetic field *y*, and magnetic field *x* components do not have appreciable amplitudes, as shown in the fifth panel in Figure 7. Perturbations in these components are often associated with standing Alfvén waves and were present in all previous observations of cavity or waveguide modes outside of the plasmasphere. Their absence in this case suggests that no other wave modes were present in the observation region. When the fast and shear Alfvén modes are weakly coupled and a global mode observation is made near the magnetic equator and remote from any field line resonances, perturbations in the electric field *x* and magnetic field *y* components should be very weak [*Lee and Lysak*, 1989].

4.3. Electromagnetic Energy Transfer

[46] The Poynting vector computed from the band pass filtered data in the FAC system is shown in the sixth, seventh, and eighth panels in Figure 7. Blue lines correspond to the instantaneous Poynting vector and red lines to the time average computed with a 10 min boxcar window. The instantaneous energy transfer associated with the radial Poynting vector (sixth panel in Figure 7) is on the order of 50 nW/m^2, with a radially inward (Earthward) average energy transfer on the order of 10 nW/m^2. The Poynting vector, both instantaneous and average, is negligible for the *y* and *z* components when compared to the *x* component (seventh and eighth panels in Figure 7). These observations differ from observations of the Poynting vector associated with standing Alfvén waves, where the *z* component (field-aligned) is significant [e.g., *Hartinger et al.*, 2011]. We note that these estimates are lower bounds for the overall energy transfer rate, as we have not estimated the kinetic energy transfer rate [*Kouznetsov and Lotko*, 1995].

4.4. Time Evolution and Spatial Structure

[47] We examine the *z* component of the magnetic field observed at THA and THD in more detail in Figure 8. The traces of both probes are plotted in Figure 8a, applying a 20 point (one minute) smoothing window to reduce digitization noise and high pass filtering (frequency >2 mHz).

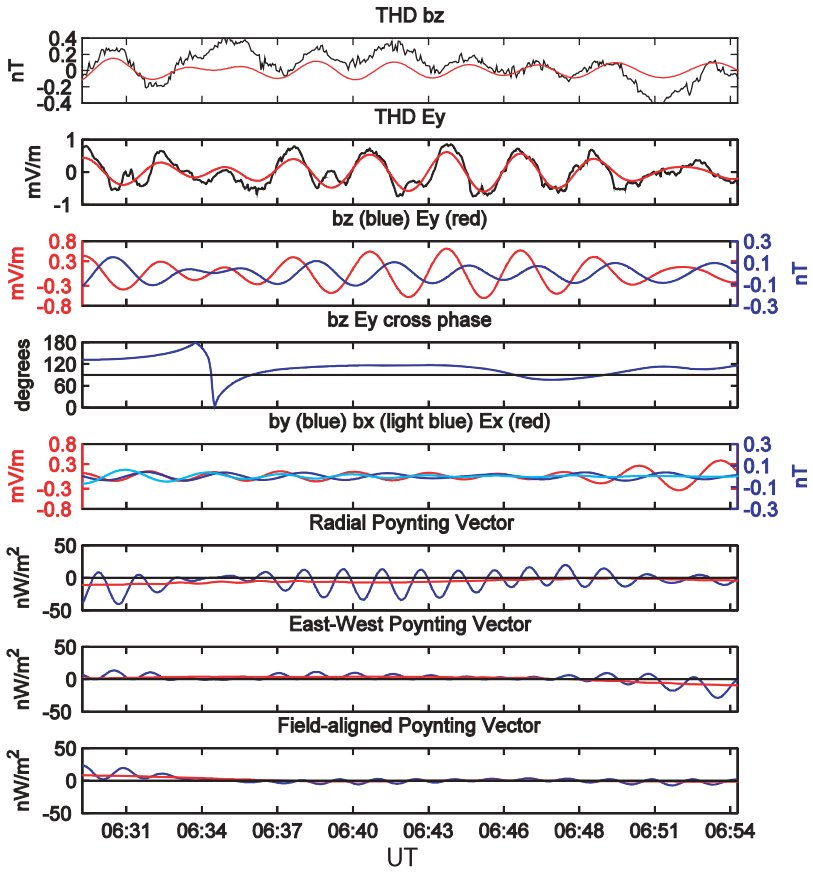

Figure 7. From top to bottom, the z component (field-aligned coordinates) of the high pass filtered (frequency >0.5 mHz) magnetic field (black) and the band pass filtered (5 < frequency <8 mHz) magnetic field (red); the same for the electric field y component; band pass filtered magnetic field z (blue) and electric field y (red) components; cross phase of magnetic field z component and electric field y component; band pass filtered magnetic field y (blue), magnetic field x (light blue), and electric field x (red) components; x component of Poynting vector from band pass filtered fields (blue) and time average (red); the same for the y component of the Poynting vector; and the same for the z component of the Poynting vector.

We verified that neither process significantly altered the phase or amplitude of the 6.5 mHz signal by comparing to the original data, as in Figure 7. THA observes the 6.5 mHz signal clearly from ~0650 to ~0730 UT. THD observes the 6.5 mHz signal intermittently throughout the interval, but a clear observation over a long period of time is made difficult by the presence of lower frequency waves seen clearly at 0630–0638 UT and 0650–0658 UT (also seen in the sixth panel in Figure 6). Both probes observe these lower frequency signals, but they have lower amplitudes when THA observes the 6.5 mHz signal, making the observation of that signal clearer.

[48] The amplitude of the 6.5 mHz signal varies for both probes throughout the interval. We examine the temporal variation of the 6.5 mHz signal by using the power spectral density from Figure 6 averaged over the frequency band from 5.5 to 8 mHz (demarcated by the black arrows in Figure 6). We compute the square root of the averaged PSD for each probe and normalize it to the maximum value observed by both probes during the interval (i.e., only one number is used for the normalization of both probes for the entire interval); this quantity is equivalent to the normalized root mean squared (RMS) amplitude. In Figure 8b, we show the normalized RMS amplitude of the z component of the perturbation magnetic field as a function of time for THA and THD. The maximum values observed by both probes are nearly equal, so the maximum value both probes observe after normalization equals or is very close to one. The amplitude of the z component perturbations at 6.5 mHz observed at THD is higher than THA at the beginning of the interval, then becomes higher at THA at ~0650 UT, and then becomes higher again at THD at the end of the interval.

[49] We next investigate whether the amplitude of the 6.5 mHz signal is changing due to spatial variations as well as temporal variations. For each PSD data point, we use the ONERA software to compute the radial distance of the magnetic equatorial crossing of the field line that the THEMIS probe is located on, which we refer to as L. The data are ordered by L in Figure 8c and have been normalized in the same manner as Figure 8b. Both probes pass through minima in amplitude at an L of 8.7 Re and subsequently see an increase in amplitude as they continue outward, suggesting there is a persistent minima in amplitude there. THD sees increased amplitude at the beginning of the interval,

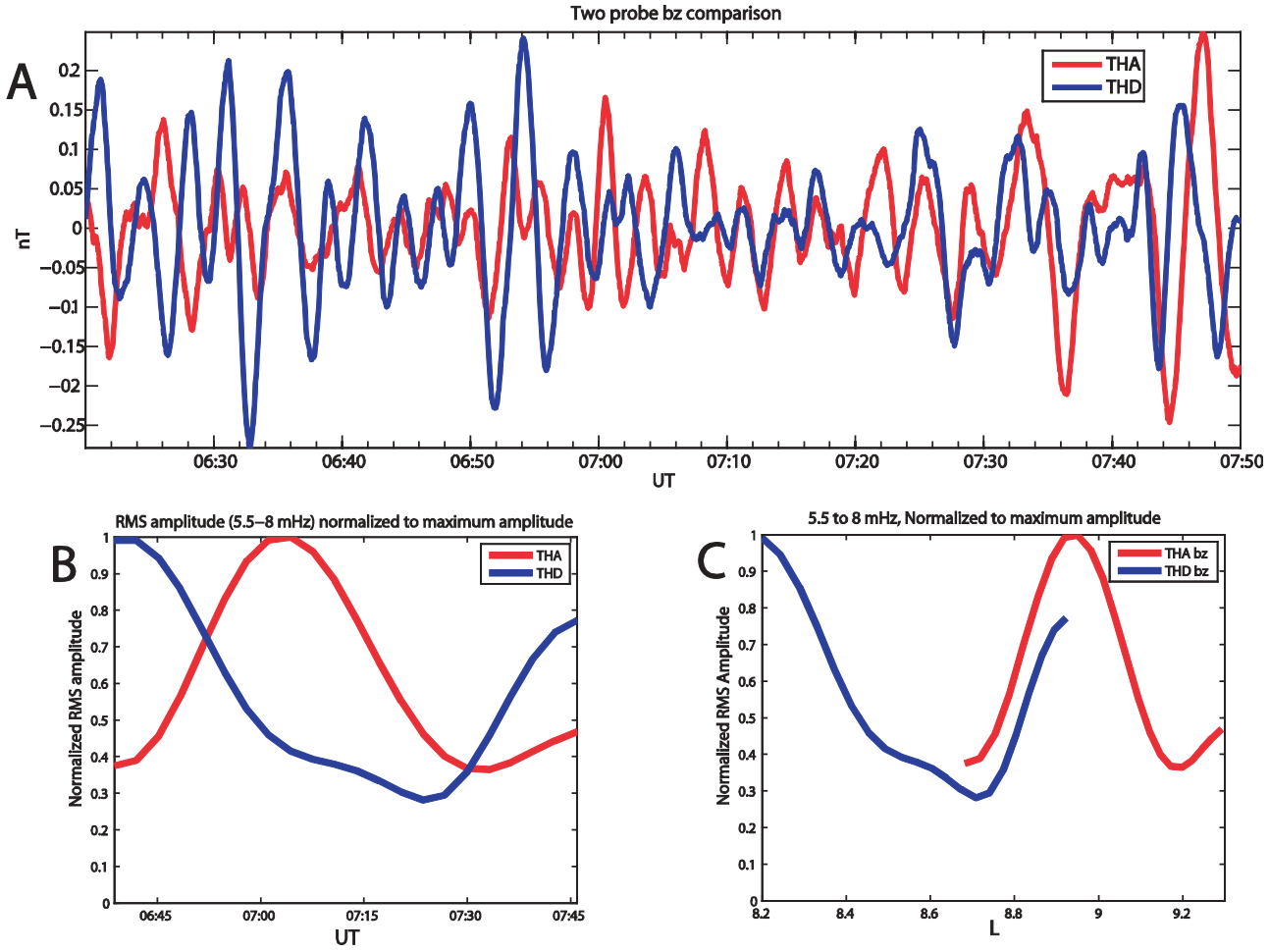

Figure 8. (a) The *z* component of the high pass filtered (frequency >2 mHz) magnetic field for THA (red) and THD (blue). Note that there are at least two signals present, one with a frequency of 4 mHz seen most clearly by THD (see section 6.5 for discussion of this signal), and one with a frequency of 6.5 mHz seen by THD and THA that we identify as a global mode. (b) The normalized root mean square amplitude of the *z* component of the magnetic field for THA (red) and THD (blue) in the 5.5 to 8 mHz frequency band. (c) The same data in Figure 8b ordered by L (radial distance).

followed by decreased amplitude, and then increased amplitude again. These observations are consistent with a radial standing wave structure, such as a global mode, which could have multiple maxima (anti-nodes) and minima (nodes) throughout the radial extent. The structure appears to be stable, as THD observes almost the same RMS amplitude as THA when it passes through the same region ~50 min later (note that observations from THD and THA are normalized to the same value). *Wright and Rickard* [1995] have previously shown that global modes can act as reservoirs for energy supplied by a time variable driver. In this case, even if the energy supplied by a driver with a broadband frequency spectrum is varying in time, a stable standing wave structure is still possible.

[50] We note here that we constructed additional figures in the same manner as Figures 8b and 8c using FFT windows of different lengths to test whether these features were artifacts of the Fourier analysis. These tests were motivated by the presence of the additional wave activity with a frequency of 4 mHz, which is close to the frequency band of interest for the global mode and raises concerns that we cannot adequately discriminate between these signals in the frequency domain. We tried a shorter FFT window (~25 min) and a longer FFT window (~100 min). Shortening the FFT window leads to less resolution in the frequency domain; in the case of the 25 min window, we observed the same peak locations as the 50 min window as well as additional peaks corresponding to periods when the 4 mHz signal was stronger. We concluded that this window was too short to adequately discriminate between the 4 mHz and 6.5 mHz signals; inspection of power spectra at times when the 4 and 6.5 mHz signal were both present also demonstrated this.

[51] In the case of the longer, 100 min window, the peaks were wider but located at the same positions as in Figure 8c. Furthermore, inspection of power spectra for the longer FFT window revealed that the 4 and 6.5 mHz signal were effectively isolated. However, both probes observed an increase in wave power at the end of the interval in the analog of Figure 8b owing to the effects of the FTE discussed in section 3.5. The ULF response to the FTE was captured by the longer window, which extended well past the end of our global mode analysis interval (see section 3 for a discussion

explaining why we selected this particular analysis interval). To avoid including effects from these later intervals, we chose to use the 50 min rather than the 100 min FFT window for our analysis. We conclude that although there may be some intervals when the 50 min window cannot completely separate the 4 and 6.5 mHz signals, we are confident that the peak locations shown in Figures 8b and 8c are not artifacts of the Fourier analysis. We obtained the same peak locations when using the longer FFT window, which can effectively isolate the 6.5 mHz signal for the entire analysis interval.

[52] We cannot exclude the possibility that the wave activity that we are observing is evolving rapidly in time, precluding the observation of the nodal structure. For example, the radial amplitude profile of a global mode depends on, among other things, the locations of the inner and outer boundaries of the cavity/waveguide. If the location of these boundaries changes in time, the peaks in amplitude associated with the global mode may shift, the width of peaks may expand/contract, or the peaks may completely disappear. It is possible that the global mode in this case was evolving in such a way that the observations from THD and THA were not adequate to observe the radial amplitude profile, and the profile shown in Figure 8c is a mixture of various profiles during the evolution of the global mode. We thus regard Figure 8c as suggestive evidence of a persistent radial profile rather than definitive proof.

[53] One of the expected features of a global mode is a 180 degree phase difference across a node, or minima, in amplitude. Inspecting the traces in Figure 8a reveals that the phase relationships between THA and THD are complicated by the presence of lower frequency waves (also seen in Figure 6). The only interval we can identify where both probes are primarily observing the 6.5 mHz signal is between 0710 and 0730 UT, where the traces appear to be in phase. This implies that THD had crossed a node at 0710 UT. Prior to 0710 UT, we cannot identify as long an interval where the 6.5 mHz signal is the main signal being observed by both THA and THD; however, there are a few shorter intervals where this is the case, such as 0626–0632 UT, where a 180 degree phase difference is observed.

[54] We note that we cannot compare the phases of these two signals using band pass filtered data and a Hilbert transform as in Figure 7, nor can we conduct cross phase analysis between the two spacecraft for the perturbations in the z component as suggested by, for example, *Waters et al.* [2002], because of the close spacing of these two frequencies and the rapid motion of the two probes through spatial structures. This exemplifies a difficulty in observing a 180 degree rotation in phase across a node of a global mode using two spacecraft. There may be other frequencies present, such as a harmonic of the global mode, that require data from a long time interval to isolate in the frequency domain. However, both spacecraft may move a significant radial distance during the longer time interval, with one or both spacecraft perhaps crossing one or more nodes of the global mode. In this particular case, we required at least a ~50 min FFT window to separate the signals with frequencies below 4 mHz from the 6.5 mHz signal. In Figure 8b, one can see that both probes are on either side of the nodal structure for only ~15 min; this is far too short a time to isolate the 6.5 mHz frequency and observe a 180 degree phase difference in the frequency domain using typical forms of cross-phase analysis (e.g., Fourier or wavelet analysis). It is also too short for filtering that could effectively separate a 6.5 mHz signal from a 4 mHz signal.

4.5. Relationship Between Wave Activity and Electron Density

[55] We finally investigate the relationship between ULF wave activity and electron density using observations from THA (red), THD (blue) and THE (green). In Figure 9a, we show electron density inferred from spacecraft potential as a function of L, or radial distance, from the three probes. All three probes are on nearly the same orbit, with THA leading THD by about 50 min, and THD leading THE by about 90 min. The plasmapause moved outward and became more structured between the time that THD and THE observed it. The time interval that the global mode was observed is indicated on this plot using bolded lines; THA and THD were outside the plasmasphere when the global mode was observed, while THE was inside the plasmasphere or at the highly structured plasmpause region.

[56] The plasmapause moved outward between the time that THD and THE observed it, as shown in Figure 9a. The timescale for this change is $\leq$2 h, too short to be explained by typical plasmaspheric refilling rates [*Darrouzet et al.*, 2009]. However, the timescale is consistent with an azimuthally structured plasmapause. In particular, if the plasmapause was more structured and located at a higher L shell at a pre-dawn local time when THA and THD observed the plasmapause at dawn, it could then drift into the dawn sector by the time that THE observed the plasmapause [*Darrouzet et al.*, 2009]. The structure, both azimuthal and radial, of the plasmapause can play a role in determining which, if any, global modes are established in the magnetosphere [*Lee and Kim*, 1999; *Lee and Takahashi*, 2006]. It is thus important to determine the role that the structure of the outer plasmasphere played in establishing the global mode observed by THD and THA. Unfortunately, the observations of the plasmapause structure that THD and THE make are widely separated in time (~0510 and ~0720, respectively), and there are several other important changes that occur during this time interval that likely played a role in establishing the global mode; most importantly, the change in the dominant driver of ULF waves and the change in the orientation of the IMF (Figures 3 and 5). Without more detailed information about the time evolution and global structure of the outer plasmasphere, we cannot separate the effects of the plasmapause structure from these other effects. It is thus beyond the scope of the present study to determine the role of these changes in the plasmapause in setting up the global mode. However, we can at least say that the plasmapause structure that THE observed was conducive to setting up global modes, as THA and THD observed the signature of the global mode at the same time that THE observed the plasmapause at approximately the same magnetic local time sector.

[57] In Figure 9b, we show the high-pass filtered (frequency >2 mHz) magnetic field y component (blue) and electric field x component (red) in the FAC system observed by THE on the same plot as electron density (black) as a function of time for the interval from 0600 to 0800 UT. The magnetic field perturbation has been scaled up by a factor of 3 to better show the time dependence of wave activity and

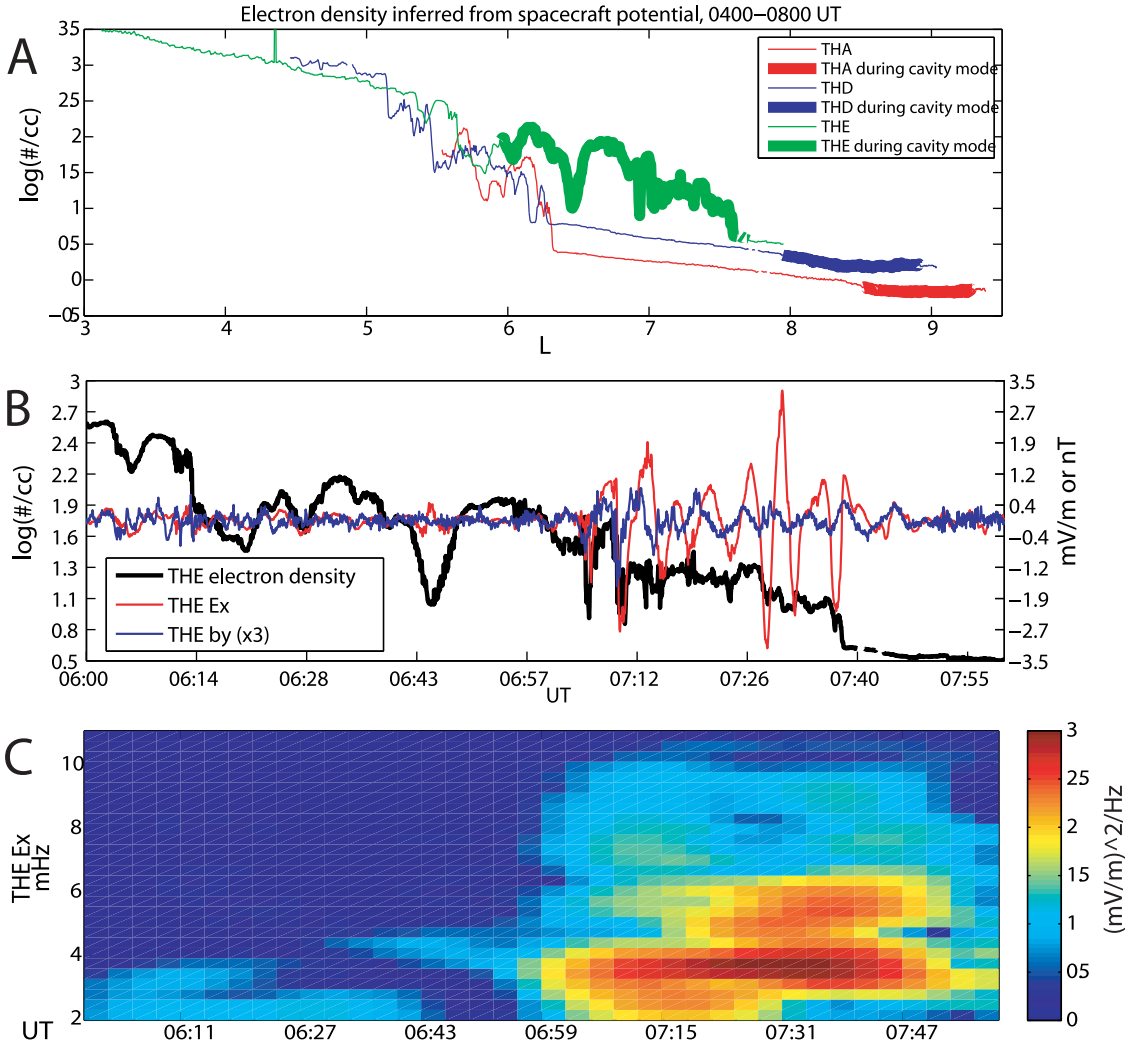

Figure 9. (a) The electron density (inferred from spacecraft potential) observed by THA (red), THD (blue), and THE (green), plotted versus L. The bolded intervals indicate observations from the period when the global mode was observed, 0625–0745 UT. (b) The electron density observed by THE (black line), the high-pass filtered (frequency >2 mHz) east-west magnetic field perturbation observed by THE (blue), and the high-pass filtered (frequency >2 mHz) radial electric field perturbation observed by THE, all plotted versus time. Note that the magnetic field perturbation has been multiplied by a factor of 3 to better see the phase difference with the radial electric field. (c) Dynamic power spectrum for the radial electric field perturbations observed by THE.

relationship with the electric field. The amplitude of wave activity is very small inside the high density region but increases sharply at ~0710 UT near the plasmapause, which we define as the point after which the electron density decreases monotonically (apart from small scale variations). We note that these are the relevant perturbations for standing Alfvén waves driven by global modes [*Kivelson and Southwood*, 1985]. In Figure 9c, we show the dynamic power spectra for the x component of the electric field; the perturbations cover a broad range of frequencies that overlap with the global mode frequency (6.5 mHz) but are peaked at lower frequencies. Further investigation of Figure 9b shows that the perturbations with largest amplitude exhibit a 90 degree phase difference between the x component of the electric field and y component of the magnetic field, as expected for standing shear Alfvén waves.

[58] We note here that there are several ways that the observed frequency of Alfvén waves can be shifted in the spacecraft frame relative to the stationary frame when a spacecraft is moving through a phase-mixed Alfvén wave structure. These frequency shifts are separate from Doppler shift, which is negligible for both the global mode and Alfvén waves in this study because the spacecraft velocity is significantly less than the wave phase velocity (whether Alfvén or fast magnetosonic). They depend on the radial velocity of the spacecraft and the rate of change of the frequency of standing Alfvén waves with radial distance [*Anderson et al.*, 1989]. These frequency shifts should not be significant, even near the plasmapause where the rate of change of the standing Alfvén wave frequency ought to be

largest. The reason is that the Alfvén waves are being continually excited by the global mode, and they do not have time to phase mix significantly. However, even if a large phase-mixing timescale is assumed, these shifted frequencies should not deviate from the stationary frame by more than about 10% when THE crosses the structured (compared to THA and THD observations) plasmapause [*Anderson et al.*, 1989]. Even if such shifts, which would only apply to Alfvén waves and not the global mode, are present, they would not affect the main conclusions of this study.

4.6. Summary of Wave Properties

[59] To summarize, using two probes we have identified wave activity outside of the plasmapause at 6.5 mHz that exhibits radial-nodal spatial structure, dominant perturbations in the east-west electric and field-aligned magnetic field, and a 90 degree phase difference between the electric and magnetic field perturbation. Furthermore, this wave activity is associated with net earthward electromagnetic energy transfer. At the same time, using a probe first located in the plasmasphere and then crossing out a highly structured plasmapause, we identify no significant wave activity in the plasmasphere followed by an abrupt increase at the plasmapause. This wave activity is spread over a large frequency range that overlaps the global mode frequency. Finally, this wave activity includes perturbations with phase relationships expected for standing Alfvén waves driven by energy transferred earthward from the global mode.

5. ULF Wave Modes That Are Inconsistent With Observations

[60] In the following sections, we compare our observations between 0625 and 0745 UT with previous observations and theory pertaining to wave modes which may be driven in the Pc5 frequency range in this region of the magnetosphere, excluding global modes. We focus on the following drivers of ULF waves that may have a compressional magnetic field perturbation, as they could operate in this region of the magnetosphere: drift-bounce resonance with ring current ions [*Southwood et al.*, 1969], the drift-mirror instability [*Hasegawa*, 1969], magnetopause surface waves driven by the Kelvin-Helmholtz instability [*Chen and Hasegawa*, 1974], and monochromatic fluctuations in the solar wind [*Kepko et al.*, 2002].

5.1. Compressional Waves Driven by Drift-Bounce Resonance

[61] Drift-bounce resonance can occur when a significant population of hot ions is available to supply energy to ULF waves that have appropriate frequencies for the resonance. *Southwood et al.* [1969] showed that waves generated through the resonance would most likely have odd symmetry about the magnetic equator with regard to field line displacement and be associated with a strong radial magnetic field perturbation at the magnetic equator. In the event presented in this paper, the radial magnetic field perturbation is significantly weaker than the field-aligned magnetic field perturbation at the magnetic equator (Figures 6 and 7), inconsistent with theory.

[62] Ion fluxes ought to rise and fall at the wave frequency for energies close to the drift-bounce resonant energy. Furthermore, there ought to be a 180 degree phase difference between flux observations above and below the resonant energy [*Southwood and Kivelson*, 1981]. Finally, overall enhancements or decreases in wave energy ought to be associated with significant changes in the ion population, as would occur during a substorm injection or the recovery phase of a geomagnetic storm [e.g., *Yang et al.*, 2010]. In the first panel in Figure 10, we show an ion energy flux spectrogram generated by the ESA and SST instruments on THD that includes energy ranges typically considered for drift bounce resonance [e.g., *Korotova et al.*, 2009]. We find that there is a general decrease in the ion energy flux with time, with one peak occurring at ~4 keV. We do not find any modulation of fluxes at the wave frequency of 6.5 mHz at any energy range, nor do we observe a 180 degree phase difference across any energy range. However, we do not stress this as definitive evidence against the drift-bounce resonance, as these features may not always be observed [*Southwood and Kivelson*, 1981; *Yang et al.*, 2010]. However, we do stress that there is no change in the overall ion population that could explain the time dependent wave activity observed by THD (Figure 6).

[63] Finally, the drift bounce resonance mechanism is not consistent with the correlation between solar wind dynamic pressure fluctuations and ULF wave power observed on the ground (Figure 3c). To summarize, the polarization of the observed waves, the lack of any time variation of ion energy flux consistent with time variable wave activity, and the relationship between dynamic pressure fluctuations and ULF wave activity observed on the ground all argue against drift bounce resonance as a viable mechanism for driving ULF waves. We conclude that drift-bounce resonance was not the driver of the 6.5 mHz wave activity for this event.

5.2. Compressional Waves Driven by the Drift-Mirror Instability

[64] The drift-mirror instability can drive ULF waves when the plasma beta, or ratio of thermal to magnetic pressure, is large and there is significant pressure anisotropy [*Hasegawa*, 1969]. Several observations of compressional waves that have been attributed to the drift mirror instability have all shown that the plasma beta was greater than one [*Zhu and Kivelson*, 1994; *Korotova et al.*, 2009]; in contrast, we observe the plasma beta to be ~0.3 throughout the interval, as shown in Figure 10b. In Figure 10c, we plot the threshold for the mirror instability, Γ, previously used by *Korotova et al.* [2009] to demonstrate that the mirror instability was a driver of ULF waves

$$\Gamma = 1 + \beta_{\perp}\left(1 - \frac{T_{\perp}}{T_{||}}\right) < 0 \quad (1)$$

where $\beta_{\perp}$ is the ratio of the thermal pressure to the magnetic pressure perpendicular to the background magnetic field, $T_{\perp}$ is the perpendicular temperature, and $T_{||}$ is the parallel temperature [*Southwood and Kivelson*, 1993]. For the entire interval when we observe the 6.5 mHz perturbation, Γ is well above 0, closer to 0.8; this is significantly larger than Γ reported in previous studies of waves driven by the drift-mirror instability, demonstrating that the mirror instability

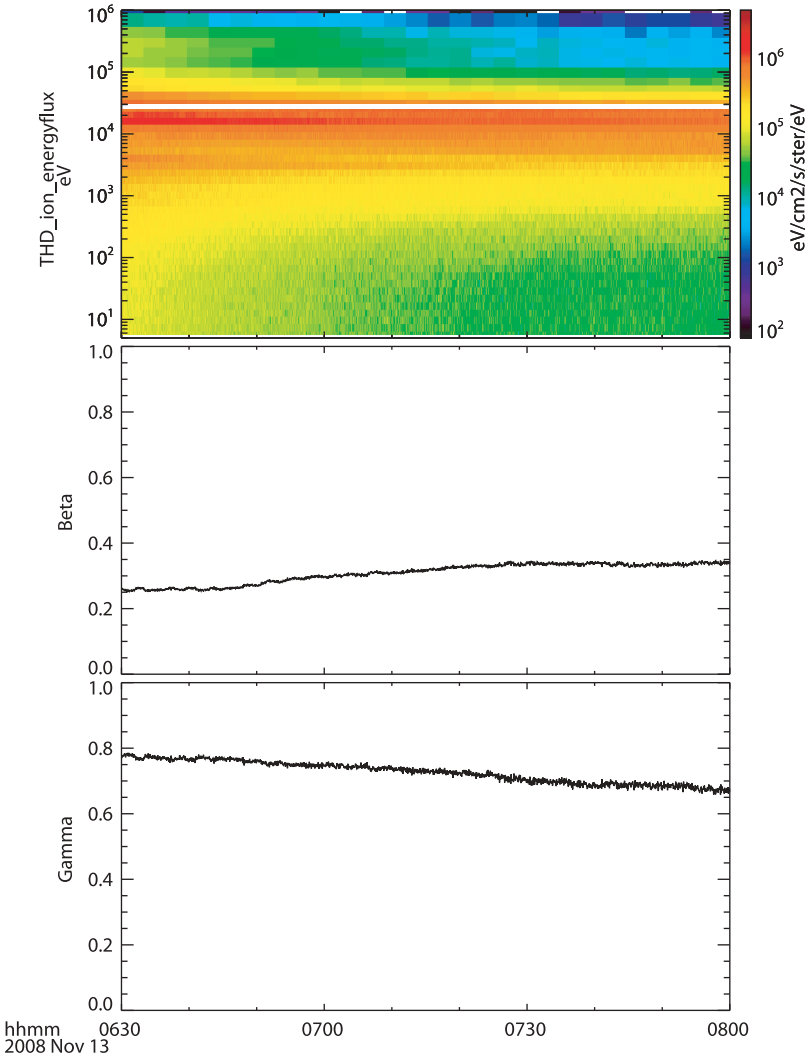

Figure 10. From top to bottom, THD ion energy flux spectrogram (measured by the ESA and SST instruments), plasma beta (ratio of thermal pressure to magnetic pressure) measured, and Γ, a parameter that indicates the threshold for the mirror instability is met when it is less than 0.

could not be driving the 6.5 mHz fluctuation [*Korotova et al.*, 2009].

[65] Waves driven by the drift mirror instability ought to have strong perturbations in the transverse magnetic field components near the magnetic equator and weak or non-existent perturbations in the field-aligned magnetic field [*Cheng and Lin*, 1987]. In some cases, the compressional perturbations may occur at the magnetic equator as a second harmonic of the transverse perturbations [*Takahashi et al.*, 1990]. However, we observe significant perturbations in the field-aligned magnetic field near the magnetic equator and comparatively small or non-existent perturbations in the transverse components both at 6.5 mHz and at lower/higher frequencies (Figure 6). Finally, like the drift bounce resonance mechanism, the drift-mirror instability mechanism is not consistent with the correlation between solar wind dynamic pressure fluctuations and ULF wave power. We conclude that the drift-mirror instability was not the driver of the 6.5 mHz wave activity for this event.

5.3. Magnetopause Surface Waves

[66] Surface waves driven by velocity shear at the magnetopause can be observed as monochromatic, compressional perturbations in the magnetosphere [e.g., *Fujita et al.*, 1996; *Agapitov et al.*, 2009; *Hartinger et al.*, 2011]. In these cases, a probe located near the magnetopause or in the magnetosheath may observe the signature of the surface wave activity in the form of multiple magnetopause crossings. In this event, THC is located in the magnetosheath and does not observe surface wave signatures, as was the case in previous magnetosheath observations that have been linked with ULF wave activity in the magnetosphere [e.g., *Agapitov et al.*, 2009; *Hartinger et al.*, 2011]; however, this evidence alone does not preclude the possibility that a surface wave is present, as the boundary undulations may have too small an amplitude for THC to observe. The amplitude of a surface mode would be expected to decay monotonically with increasing distance from the magnetopause [*Chandrasekhar*, 1961]. In this event, the wave amplitude is higher at a probe (THD) that is further from the magnetopause than another

probe (THA) during part of the interval, inconsistent with a surface wave. Finally, there should be some net energy flux tailward for a magnetopause surface wave [*Junginger*, 1985]; during several parts of the interval of interest in this event, there is extremely weak or non-existent tailward energy flux (Figure 7). We conclude that magnetopause surface waves were not the driver of the 6.5 mHz wave activity for this event.

5.4. Compressional Waves Directly Driven by Monochromatic Dynamic Pressure Fluctuations

[67] Monochromatic fluctuations in the solar wind have been directly linked to compressional ULF wave in the magnetosphere with the same frequency, with typical frequencies that are comparable to or less than 2 mHz [*Kepko et al.*, 2002; *Viall et al.*, 2009]. In this event, there is evidence of fluctuations in the solar wind dynamic pressure at ~2 mHz that may be driving ULF waves of the same frequency in the magnetosphere. However, fluctuations at higher frequencies in the magnetosphere do not appear to be directly correlated with monochromatic fluctuations in the solar wind (Figure 6). Furthermore, it is unlikely that monochromatic fluctuations in the solar wind could generate the persistent nodal structures observed by THA and THD. Finally, a frequency of 6.5 mHz is above expected frequencies for quasi-static driving of the magnetosphere by solar wind dynamic pressure fluctuations [e.g., *Kepko and Spence*, 2003]. We conclude that dynamic pressure fluctuations are not directly driving the 6.5 mHz ULF waves observed at THD and THA, although broadband dynamic pressure fluctuations provide a source of energy for these waves.

6. Global Mode Driven by Broadband Dynamic Pressure Fluctuations

[68] Using geomagnetic activity indices and observations in the solar wind, magnetosheath, magnetosphere, and on the ground, we identified an interval favorable for observing a global mode on 13 Nov 2008 from 0625 to 0745 UT. The criteria we used for selecting the interval was the availability of in situ and ground observations in nearly the same local time sector and in a radial alignment, a stable magnetopause location (based on steady, northward IMF and no large changes in solar wind dynamic pressure), the ability to identify a single driver of ULF waves (broadband dynamic pressure fluctuations), and no significant transient ULF wave activity. We used data from the THEMIS probes and on the ground to identify the properties of ULF waves during this interval. Using these data, we examined the possibility that these waves could be generated by several mechanisms which are known to produce monochromatic fluctuations in the Pc5 frequency range: drift-bounce resonance, drift-mirror instability, magnetopause surface waves, and monochromatic fluctuations in the solar wind. Having eliminated these mechanisms as potential drivers of the monochromatic wave activity, we now examine the global mode mechanism as a means of generating these waves.

6.1. Expected Global Mode Features

[69] It is expected that global modes should have field-aligned magnetic field perturbations and east-west electric field perturbations that are 90 degrees out of phase, as observed in this event (Figure 7) [*Waters et al.*, 2002]. These perturbations were dominant for much of the event, consistent with a wave standing primarily in the radial direction. Global modes should also exhibit a distinct nodal structure throughout their radial extent, as expected for a radially standing wave and as was observed in this event (Figure 8c). Finally, dynamic pressure fluctuations are strongly correlated with ULF wave activity in the magnetosphere, suggesting that they could provide a source of energy for wave activity (Figure 3c). However, dynamic pressure fluctuations exhibit a broadband frequency spectrum above 2 mHz, yet compressional magnetic field perturbations in the magnetosphere are monochromatic (Figure 6). The global mode mechanism provides a ready explanation for this discrepancy. *Wright and Rickard* [1995] showed that drivers with a broad frequency spectrum can excite global modes at discrete frequencies; these global modes can act as reservoirs of energy, maintaining a stable spatial structure even when the rate that energy is supplied by the driver varies in time. Based on these lines of evidence, and the evidence eliminating the possibility for other typical sources of wave activity that have compressional magnetic field perturbations, we conclude that the 6.5 mHz fluctuation observed at THA and THD was a global mode.

6.2. Coupling Between Global Mode and Shear Alfvén Waves

[70] In certain cases, standing fast mode waves can couple to shear Alfvén waves. For this to occur, the global mode must match the standing Alfvén wave frequency at some location in the magnetosphere [*Kivelson and Southwood*, 1985; *Allan et al.*, 1986b; *Wright and Rickard*, 1995]. Additionally, *Kivelson and Southwood* [1985] showed that global modes are evanescent through some of their radial extent before they couple to shear Alfvén waves at the location where the global mode frequency matches the standing Alfvén wave frequency. *Zhu and Kivelson* [1989] and others have shown that the energy transported to a standing Alfvén wave from a global mode depends on the distance between the point where the global mode becomes evanescent and the point where the frequencies are matched. We have presented evidence in Figure 9 that standing Alfvén waves were excited near the plasmapause. In Figure 11, we examine the relationship between these Alfvén waves and the global mode using qualitative comparisons with the numerical model of a cavity mode (a type of global mode) from *Zhu and Kivelson* [1989]; the qualitative results of this model can also be applied to other global modes, such as waveguide modes [*Wright*, 1994; *Rickard and Wright*, 1994].

[71] In Figure 11a, we show the magnetic field z perturbation (blue), associated with the cavity mode, and the electric field x perturbation (red), associated with Alfvén waves, generated from the model. One cavity eigenfrequency is shown for a case where the Alfvén speed varies as distance$^{-3/2}$, which is expected for a dipole magnetic field and density variations as in *Carpenter and Anderson* [1992]. The nodal structure of the cavity mode is seen in the outer region, and it rapidly decreases with decreasing radial distance at the same location as the Alfvén wave activity is sharply peaked (~6.8 Re). In Figure 11b, we show observations of the magnetic field z perturbations in the 5.5 to

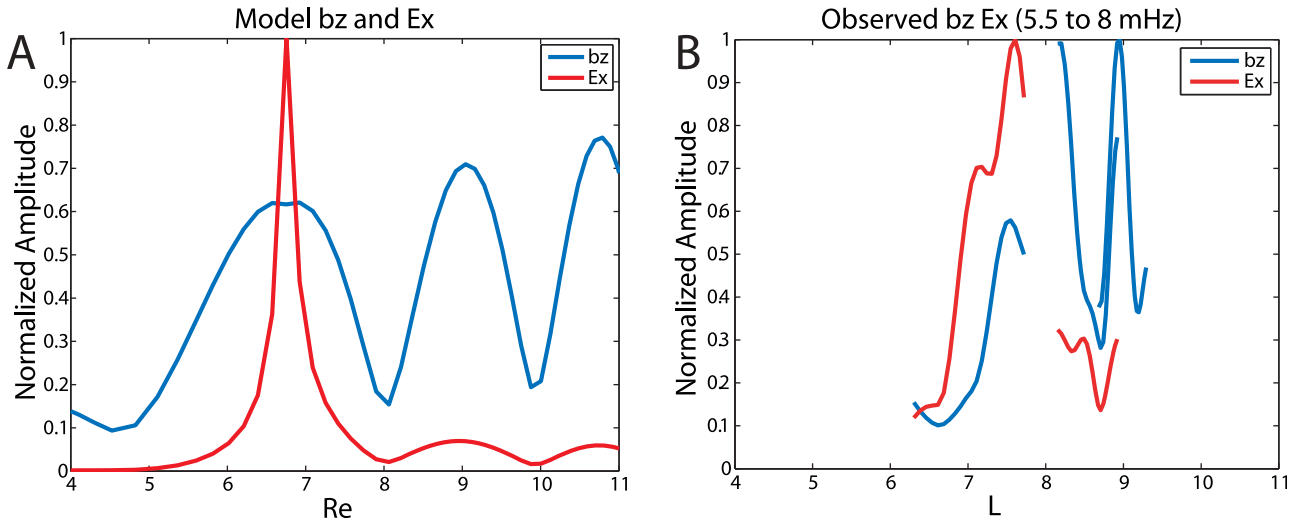

Figure 11. (a) The z component of the magnetic field perturbation (blue) and x component of the electric field perturbation (red) for a global mode generated using the *Zhu and Kivelson* [1989] 1D model. The x axis indicated distance from the inner model boundary. One eigenfrequency is shown for a case where the Alfvén speed varies as distance$^{-3/2}$, which is expected for a dipole magnetic field and density variations as in *Carpenter and Anderson* [1992]. (b) The same as Figure 11a, but for observations from THA, THD, and THE between 0625 and 0745 UT. These data are plotted versus L, or radial distance.

8 mHz frequency band (blue) and electric field x perturbations in the same frequency band from THA, THD, and THE, normalized in the same manner as in Figure 8. In particular, the magnetic field perturbations from each probe are all normalized to the maximum value observed by all three probes during the entire interval (i.e., only one number is used for normalization), and the same is done for the electric field perturbations (note that we have excluded the electric field data from THA because of contamination – see Appendix A and auxiliary material). Qualitatively similar results are seen between the model and observations; namely, nodal structure from the magnetic field z component in the outer region where the electric field perturbations are weak and strongly enhanced radial electric field perturbations in the inner region where the global mode frequency matches the standing Alfvén wave frequency. This, combined with the radially inward energy transfer observed in the outer region (Figure 7), suggests that a global mode is driving shear Alfvén waves during this event. We note the observations show narrower magnetic field peaks than the numerical model; more recent models have shown similarly narrow peaks [e.g., *Waters et al.*, 2002].

[72] The model should only be used for qualitative comparisons because we have not included the sharp changes in plasma mass density at the plasmapause. Such sharp changes can play an important role in coupling between global modes and shear Alfvén waves [e.g., *Zhu and Kivelson*, 1989]. In particular, the frequency of standing Alfvén waves changes rapidly at the plasmapause, which can in turn lead to a large range of different frequencies being excited over a small radial distance, perhaps explaining the broad range of frequencies seen by THE as it crosses the plasmapause (Figure 9c) [*Lin et al.*, 1986]. A plausible scenario to explain the coupling between global modes and shear Alfvén waves at the plasmapause in such cases could include the frequency of the fundamental and perhaps additional harmonics of a cavity mode all matching standing Alfvén wave frequencies near the sharp density gradient. Alfvén waves would then be excited at one or more frequencies over a small radial distance and phase mix [e.g., *Mann et al.*, 1995]. This would lead to enhancements in wave power at a broad range of frequencies at the plasmapause that are similar to the global mode frequency or frequencies, rather than exactly matching the discrete frequencies of the global mode. Finally, we note that there may be small differences between the data shown in Figure 11b, which was measured in the moving spacecraft frame, and data transformed to a stationary frame. These small differences are discussed in section 4.5, and they will not affect the qualitative comparison with the model shown in Figure 11a.

6.3. Cavity or Waveguide Mode

[73] Throughout this study we refer to the standing fast mode waves that THA and THD observe as a global mode. In this section, we discuss the relevance of models of two types of global modes, cavity and waveguide modes, to our observations. We emphasize that whether the observations are better described as cavity or waveguide modes, the main conclusions of this paper remain unchanged: broadband dynamic pressure fluctuations can excite global modes (whether cavity or waveguide modes) outside the plasmasphere and in the Pc5 frequency range, and these global modes can in turn excite standing Alfvén waves.

[74] Cavity models treat the magnetosphere as a closed system, with energy only allowed to leak into the ionosphere. In these models, cavity modes have discrete azimuthal wave numbers and extend to all azimuthal locations [e.g., *Kivelson and Southwood*, 1985]. In the present study, we do not have enough observations to conclude that the global mode is present at all azimuthal locations. Also, the spacecraft configuration is not ideal for estimating the azimuthal wave number (due to their small azimuthal

separation and rapid motion through spatial structures - see section 4.4). However, the monochromatic compressional magnetic field perturbations, polarization, and nodal structure are all consistent with cavity mode theory.

[75] Several authors have proposed that the flank magnetosphere is better described as a waveguide than a cavity, as energy leaks into the tail, leading to dispersion and wave modes with a continuum of azimuthal wave numbers. In our event we did not observe significant tailward energy transfer (seventh panel in Figure 7), nor were our observations consistent with a broad frequency spectrum that was previously attributed to dispersion in the flank waveguide [*Mann et al.*, 1998]. However, these observations do not preclude the possibility that the observations are of a waveguide mode. The THEMIS probes used in the present study were not in an ideal, azimuthally separated configuration to observe dispersion as in *Mann et al.* [1998]. Furthermore, if the observations are not very remote from the region on the magnetopause where driving is strongest, the THEMIS probes would observe a waveguide mode with low azimuthal wave number. The waveguide mode observations would be identical to those expected for a cavity mode, although energy would be propagating away from the location of the THEMIS probes and down the waveguide, inconsistent with cavity mode theory [e.g., *Wright*, 1994].

[76] The observations that we have presented could be consistent with either a cavity mode or a waveguide mode with low azimuthal wave number. Although we lack the observations to definitively categorize the global mode as either a cavity or waveguide mode, we find that waveguide mode theory is an appealing description of the manner in which global modes can be excited in the outer magnetosphere (i.e., outside the plasmasphere), in that it includes the possibility that wave energy can leak into the magnetotail and allows for a continuum of azimuthal wave numbers.

6.4. Global Mode Boundaries and Frequency

[77] We note that the frequency of the global mode was in the Pc5 band, and that it was observed at large L shells (L > 7), where Pc5 FLRs are often observed. Examination of the electron density profiles inferred from spacecraft potential reveals that the plasmapause was located at L ~ 7 when the global mode was observed, and that THE was inside the plasmasphere whereas THD and THA were outside the plasmasphere (Figure 9a). We do not have the data coverage to identify the exact location of the inner boundary of the cavity. However, our observations strongly suggest that the plasmapause is the inner boundary, as the wave amplitude is significantly lower at THE compared to THD and THA (Figure 9b).

[78] It is more difficult to determine the outer boundary of the cavity, due to a lack of observations near the magnetopause. Some models and simulations of global modes have assumed or showed that the magnetopause can function as an outer boundary, whereas a few others have extended the outer boundary to the bow shock [e.g., *Samson et al.*, 1992; *Claudepierre et al.*, 2009]. In Figure 12, we show data from THB (solar wind), THC (magnetosheath), and THD and THA (magnetosphere) which suggest that the global mode may extend into the magnetosheath. Figure 12 (top) shows, from top to bottom, the high pass filtered (frequency > 1 mHz) solar wind dynamic pressure measured at THB, total pressure (thermal and magnetic) perturbations measured at THC, and compressional magnetic field perturbations measured at THA and THD. The 6.5 mHz signal corresponding to the global mode is seen most clearly when THD is passing through an anti-node from ~0630–0655 and when THA is passing through an anti-node from ~0645–0715. A 6.5 mHz signal can also be seen in the magnetosheath (THC, second panel in Figure 12 (top)) most clearly from ~0630–0650, yet no 6.5 mHz signal is evident in the solar wind (first panel in Figure 12 (top)).

[79] We selected two intervals for Fourier analysis to test whether there is a persistent signal in the magnetosheath related to the global mode that THD and THA observe. The intervals correspond to periods when each probe was passing through an anti-node and most clearly observed the 6.5 mHz signal (see Figure 8). We used a 512 point (26 min) FFT window for this analysis. As noted in section 4.4, this choice of window will tend to blur the 4 and 6.5 mHz signals observed in the magnetosphere; however, for the purpose of this analysis, we require a shorter FFT window to separate wave activity in time and are not concerned with resolving these signals completely in the frequency domain. In Figure 12 (bottom left), the PSD for the solar wind dynamic pressure fluctuations, magnetosheath total pressure fluctuations, and compressional magnetic field perturbations observed by THD are shown for the first interval. Each trace has been normalized to the maximum PSD. Both compressional magnetic field perturbations in the magnetosphere and total pressure fluctuations in the magnetosheath have a distinct peak in PSD at 6 mHz (a negligible difference from 6.5 mHz when considering the precision of this Fourier analysis), yet there is no peak at this frequency in the solar wind. Figure 12 (bottom right) shows data in a similar manner to Figure 12 (bottom left) from a later interval, except that data from THA is shown instead of THD. During this later interval, the total pressure perturbations observed at THC have a broader frequency spectrum, but they are still enhanced above background levels near 6.5 mHz and overlap with the peak that THA observes (corresponding to the global mode). We conclude that there is a persistent ~6.5 mHz signal in the magnetosheath that is likely related to the global mode signature at THA and THD. To our knowledge, this is the most direct evidence ever reported of global modes extending into the magnetosheath. We cannot say with certainty, however, that the global mode extends into the magnetosheath, as the global mode may be observable yet evanescent in the magnetosheath.

[80] We can obtain an estimate of the fundamental global mode frequency using a time of flight calculation (transit time for a fast mode wave from one boundary of the cavity to the other and back again)

$$f^{-1} = 2\mathrm{Re}\int_{Li}^{Lo}\frac{dL}{V_{fm}} \tag{2}$$

where f is the frequency, Re is an Earth radius, L_i is the location of the inner boundary, L_o is the location of the outer boundary, and V_{fm} is the speed of a fast mode wave [*Takahashi et al.*, 2010]. This calculation requires many assumptions, as we cannot definitively constrain the location of the inner and outer boundary and we lack observations of magnetic field, density, and temperature in a large region of

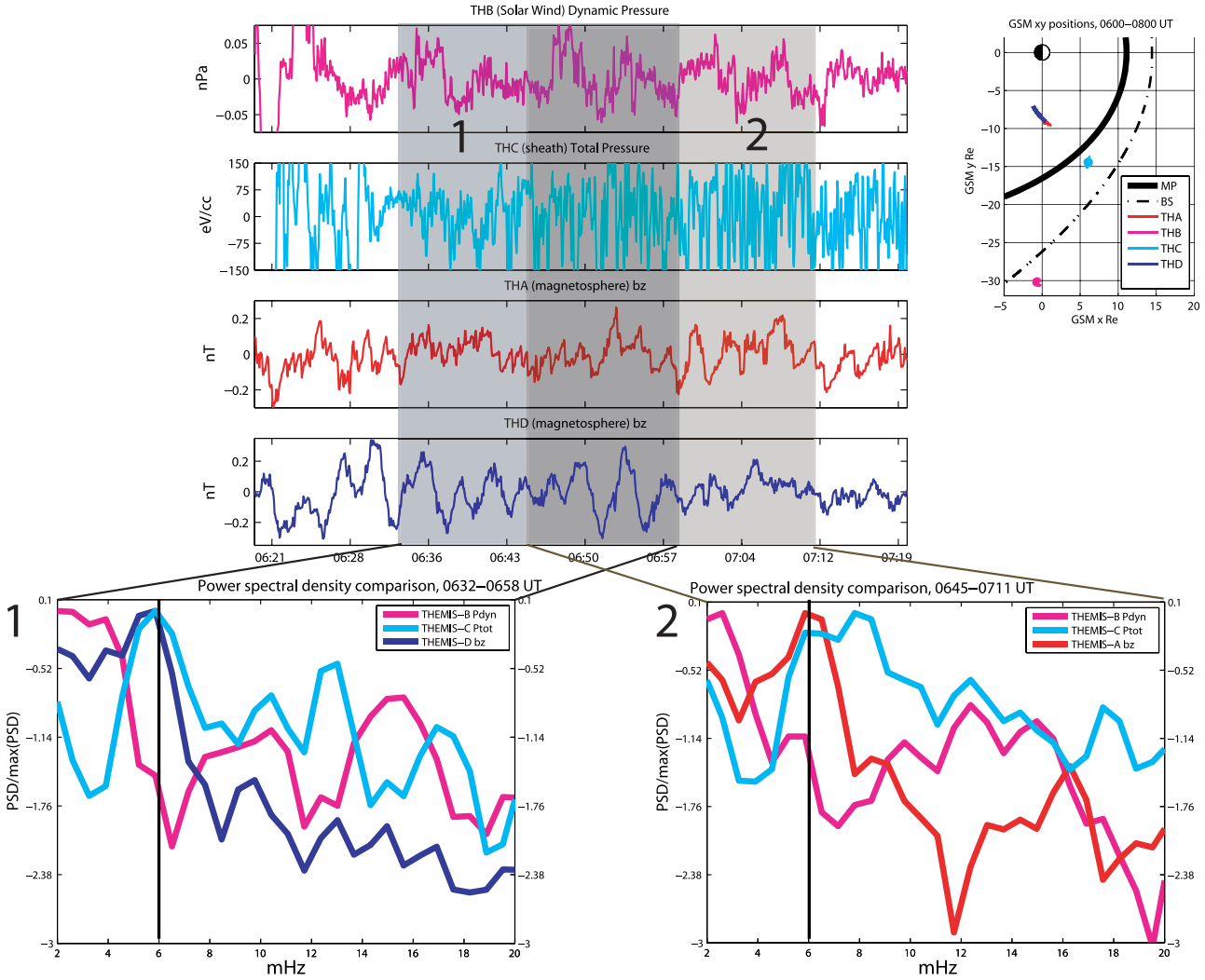

Figure 12. (top) From top to bottom, traces of the high pass filtered (frequency>1 mHz) solar wind dynamic pressure observed by THB, total pressure observed by THC, compressional magnetic field observed by THA, and compressional magnetic field observed by THD. (bottom) Corresponding intervals for Fourier analysis for the two numbered, shaded areas in Figure 12 (top). (bottom left) A comparison between PSDs for the compressional magnetic field perturbations observed by THD (dark blue), total pressure fluctuations observed by THC (light blue), and solar wind dynamic pressure fluctuations observed by THB (pink), all normalized to their respective maximum values; a black line denotes 6 mHz. (bottom right) The same but for the second interval and using THA (red) instead of THD.

the flank magnetosphere. We present two sets of assumptions that lead to different estimates of the fundamental frequency below.

[81] In the first estimate, we assume the inner boundary at the plasmapause ($L_i \sim 7$ based on observation), the outer boundary at the flank magnetopause ($L_o \sim 17$, according to the *Shue et al.* [1997] model), the temperature constant throughout the cavity, the only ion species is protons, the magnetic field varies as a dipole, and the electron density varies as $L^{-4.5}$ (based on the empirical model of *Carpenter and Anderson* [1992]). Using observations at THD during the global mode observation, we find that the Alfvén speed is ~1300 km/s (at ~0700 UT, L ~ 8) when assuming pure hydrogen or ~1000 km/s when assuming 5% oxygen, the sound speed is 600 km/s, and the fast magnetosonic speed is ~1400 km/s or ~1200 km/s, depending on ion composition. Finally, we assume that the fundamental is a quarter wavelength mode, as previously reported by *Mann et al.* [1999] and *Claudepierre et al.* [2009]. To use this assumption, we must divide the fundamental frequency from equation (2), which assumes a half-wavelength fundamental mode, by 2. With these observations and assumptions, we find that the frequency of the fundamental global mode is 3.8–4.5 mHz. A larger fraction of heavy ions in the plasma, contributions from the colder, denser plasma of the low latitude boundary layer, and an inner displacement of the inner boundary or outer displacement of the outer boundary would all significantly decrease the estimated fundamental frequency.

[82] These calculations are consistent with our observations if we assume that the 6.5 mHz global mode is a harmonic. Our observations suggest that it is a harmonic, based on the observed nodal structure (Figure 11). The separation

between the two nodes observed by THD and THA is between 0.75 and 1 Re, while the cavity that we have assumed is 10 Re wide. In the case of a homogeneous cavity with one perfectly reflecting boundary, as assumed above for the quarter-wavelength fundamental mode, the wavelength of the global mode would be 40 Re and the fundamental would have a spacing between nodes of 20 Re. The observed spacing between nodes of 1 Re would then imply that the observed wave is a twentieth harmonic; if two perfectly reflecting boundaries are assumed for a half-wavelength rather than quarter-wavelength fundamental, the observed spacing would imply a tenth harmonic wave. However, these observations do not necessarily imply that the global mode is a tenth or twentieth harmonic, since several studies have showed that the separation between nodes in an inhomogenous medium is highly irregular [e.g., *Zhu and Kivelson*, 1989; *Waters et al.*, 2002]. Furthermore, the fact that we observe a frequency that is roughly double our estimated fundamental frequency does not necessarily imply that we are observing the first harmonic (which would be inconsistent with the higher harmonic number implied by the observed radial amplitude structure) for two reasons: one is the considerable uncertainty in the estimated frequency, and the second is the fact that harmonics are not necessarily integer multiples of the fundamental frequency in an inhomogeneous medium [*Allan and McDiarmid*, 1993]. However, the small separation between nodes, when compared to the size of the cavity, is somewhat unexpected given that the estimated fundamental frequency is lower than but within a factor of two of the frequency we observe, suggesting either a first or at most a second harmonic [*Allan and McDiarmid*, 1993]. This suggests that either the nodal structure is highly irregular (i.e., very small nodal separation in this region compared to elsewhere in the cavity) or at least one of the assumptions contained in the time-of-flight calculation is not valid. These concerns remain if we assume a half-wavelength mode as the fundamental mode rather than a quarter-wavelength mode.

[83] One major assumption that we have made in the time-flight-calculation which may be invalid is the location of the outer boundary. In the second estimate of the fundamental frequency, we assume that the global mode is not bounded by the magnetopause and extends into the magnetosheath, as suggested by data shown in Figure 12. Due to the large number of assumptions that must be made to calculate the fundamental frequency in this case, we do not attempt an estimate in the same manner as our first suggested scenario. We rely instead on the results shown in *Harrold and Samson* [1992], which demonstrated that global modes that extend into the magnetosheath can have frequencies on the order of 1 mHz for typical plasma and magnetic field parameters. A fundamental frequency on the order of 1 mHz is consistent with our observations for the same reasons described for the first scenario, assuming that the global mode we observe is a harmonic of the fundamental. However, this scenario allows for the observed global mode to be a higher order harmonic than the previous scenario, as the fundamental frequency would be much lower than 3.8–4.5 mHz.

[84] We finally note that the apparent inconsistency between the observed radial amplitude structure and the observed frequency of the wave activity (implying an unrealistically high harmonic number) may be based on inaccurate observations of the spacing between nodes. As already noted in section 4.4, we cannot exclude the possibility that the global mode is evolving rapidly in time. In particular, the time required to observe the spacing between amplitude peaks, or anti-nodes, was roughly one hour (Figure 8b). This far exceeds the timescale on which the global mode may change, which is comparable to the wave period (~3 min). We have tried to identify an interval in which a global mode would be expected to be stable when selecting this event (see section 3). Despite these efforts, we still observed significant time evolution of the outer plasmasphere (Figure 9a) which could have altered the properties of the global mode and precluded an accurate observation of the spacing between nodes/anti-nodes. If this is the case, our estimate of 0.75–1 Re for the spacing between anti-nodes may not be accurate, and there may be no need to invoke higher order harmonics to explain the discrepancy between the observed frequency and an incorrectly estimated nodal spacing.

6.5. Relationship Between Global Mode and Lower Frequency Waves

[85] Both THD and THA observe perturbations at lower frequencies than 6.5 mHz. We attempted to identify the source of these waves and their relationship to the 6.5 mHz signal. As mentioned previously, it is likely that waves below 2 mHz are being directly driven by solar wind dynamic pressure fluctuations of comparable frequency. It is more difficult to identify the source of the waves between 2 and 6.5 mHz. These waves have frequencies of several mHz and are associated with enhanced east-west magnetic and radial electric field perturbations (e.g., second and fifth panels in Figure 6) during at least the latter part of the interval, all of which are consistent with standing shear Alfvén waves [e.g., *Lee and Lysak*, 1989]. If these are standing Alfvén waves, they may be unrelated to the 6.5 mHz global mode. A broadband driver, such as solar wind dynamic pressure fluctuations, can excite a continuum of standing Alfvén waves throughout the entire magnetosphere without the presence of a global mode [*Dungey*, 1967]. Thus, it is possible that the broadband solar wind fluctuations are driving Alfvén waves at frequencies that are set by the local field line resonance frequency as well as a global mode at the 6.5 mHz frequency (frequency set by the magnetospheric cavity properties).

[86] There are some features of the wave activity between 2 and 6.5 mHz that cannot be easily explained by standing Alfvén waves. In particular, there are strong z component perturbations between 2 and 6.5 mHz observed by THD between ~0630 and 0700 UT that are not observed by THA (third and sixth panels in Figure 6). Similarly, there are strong z component perturbations between 2 and 6.5 mHz observed by THA after 0730 UT that are not observed by THD (third and sixth panels in Figure 6). Standing Alfvén waves driven by the solar wind are not typically associated with strong perturbations in the z component. Furthermore, we can rule out other potential drivers of ULF wave activity with strong z component perturbations between 2 and 6.5 mHz for the same reasons that we ruled them out for the 6.5 mHz global mode. In particular, the ambient plasma conditions do not support the drift mirror instability or the drift-bounce resonance mechanisms, and the z perturbations at THD (inner probe) are much larger than at THA (outer

probe) for at least part of the interval, precluding the possibility of direct driving by a magnetopause surface wave or monochromatic fluctuations in the solar wind.

[87] These z perturbations could, however, be evidence for a global mode. An immediate question is what is the relationship between these z perturbations, the Alfvén wave activity, and the 6.5 mHz global mode. Unfortunately, further analysis of the polarization properties and spatial structure of this lower frequency wave activity to confirm the presence of a global mode in the same manner as for the 6.5 mHz fluctuations is complicated for several reasons: the 6.5 mHz signal is also present, Alfvén waves are also present, and the intervals of time in which the lower frequency signal is clearly observed are too short for detailed analysis (i.e., appropriate filtering or isolation of the signal in the frequency domain is not possible). However, it is possible that the 6.5 mHz global mode is a harmonic of a lower frequency global mode. This hypothesis is supported by the observations of large amplitude standing Alfvén wave perturbations at the plasmapause by THE, which have their peak power at a lower frequency than 6.5 mHz (Figure 9c). This lower frequency global mode could be driving Alfvén waves at the same frequency at the plasmapause.

7. Summary

[88] Unlike previous observations of global (cavity/waveguide) modes outside the plasmasphere, this study reports on observations of a global mode in the absence of other wave modes. This facilitates wave mode identification, as the small amplitudes observed ($\sim$100 pT, 0.8 mV/m) could easily have been obscured by other wave activity that can occur at similar locations with higher amplitudes, such as compressional waves driven by the drift-mirror instability [e.g., *Korotova et al.*, 2009]. Furthermore, we have presented evidence of coupling between a global mode and shear Alfvén waves; in particular, we have shown radially inward energy transfer from the global mode to the plasmapause, where shear Alfvén waves in the same frequency range as the global mode are observed. Finally, we have shown that monochromatic global mode waves can be generated outside the plasmasphere at the flank of the magnetosphere, despite the fact that substantial dispersion is expected from tailward propagation [*Rickard and Wright*, 1995].

[89] Our observations suggest that global modes are a viable mechanism for converting energy from fluctuations in the solar wind to monochromatic fluctuations in the Pc5 frequency band in the magnetosphere, even if those external fluctuations are broadband. Our results can help explain the propensity of monochromatic, Pc5-band ground pulsations to develop over a wide range of latitudes in the absence of a monochromatic solar wind driver [*Wright and Rickard*, 1995]. Moreover, a monochromatic global mode is required in order to generate monochromatic, radially localized Alfvén waves via FLR. Our results, therefore, lend observational credence to the global mode driver model of FLRs localized at mid to high latitudes, at least during the particular conditions (e.g., IMF northward) during which this event occurred [*Samson and Rostoker*, 1972; *Walker et al.*, 1979].

[90] We have not shown the relationship between a monochromatic global mode and a monochromatic standing Alfvén wave directly in this study, as we observed standing Alfvén waves with a range of frequencies that overlapped the global mode frequency; we attributed this range of frequencies to the sharp density gradient at the plasmapause. However, we have shown that monochromatic global modes can at least drive standing Alfvén waves over a frequency range that includes the global mode frequency; we expect that monochromatic Alfvén waves would be observed when driven by global modes in regions with smaller, smoother density gradients.

[91] This event was selected from a small number of similar events that occurred over a span of several months during intervals when geomagnetic activity was low, only one potential driver of ULF waves was expected to be present (to facilitate wave mode identification), and spacecraft conjunctions were ideal. A future study will include investigation of these events and a larger set of events during more varied conditions to further examine the coupling between the solar wind, cavity/waveguide modes, and shear Alfvén modes.

Appendix A: Validation of THEMIS Electric Field Data for the Measurement of ULF Waves

[92] The instantaneous phase of ULF waves observed by the THEMIS probes is of primary interest for this study. In particular, the phase difference between the east-west electric and field-aligned magnetic perturbation and the phase differences between spatially separated probes. However, measurements of ULF electric field fluctuations by EFI can potentially be contaminated by spurious, non-geophysical electric fields [*Bonnell et al.*, 2008]. The sources of these fields include electrostatic wakes generated by the motion of the spacecraft through cold plasma (e.g., the plasmasphere) and asymmetric illumination of EFI booms caused by, for example, passage through the shadow of the spacecraft [*Mozer*, 1973]. These spurious electric fields may affect the measurement of both the amplitude and phase of geophysical electric field fluctuations such as global modes. Furthermore, they may affect the spatially separated THEMIS probes in different ways. These effects will confound any attempt to identify global modes. We thus identify and remove from our analysis intervals where contamination is significant.

[93] EFI measures the electric field in the spin plane using the voltage difference between two spherical probes at either end of a 49.6 m boom and two spherical probes at either end of a 40.4 m boom. These spinning spacecraft frame electric fields are sampled 32 times per spin and both the long and the short boom electric fields can be fit separately to a model of the form

$$A + B\sin(\psi) + C\cos(\psi)$$

using a least squares method, where Ψ is the spin phase relative to the Sun pulse (when the Sun sensor is pointed at the Sun) and A, B, and C are the fit parameters. The fit parameters are then used to compute the electric field in other, non-spinning coordinate systems. This fitting procedure is routinely done on board the spacecraft, and during some intervals, referred to as "slow survey," only the fit parameters for the longer boom are returned to the ground.

However, during other intervals known as "fast survey," the voltage differences and electric fields in the spinning frame for both the short and long booms are returned to the ground.

[94] The most direct technique to identify possible sources of contamination for the electric field measurement is to inspect the voltage or electric fields measured in the spinning spacecraft frame when fast survey data are available. In the presence of a geophysical electric field that varies on a timescale much greater than one spin period (3 s), the waveforms should appear sinusoidal. Wake electric fields or asymmetric illumination of the booms will cause deviations from sinusoidal behavior (see auxiliary material or *Bonnell et al.* [2008] for examples). However, the presence of these effects does not necessarily preclude the use of EFI data. Non-geophysical spikes in the waveforms corresponding to, for example, shadowed intervals are routinely removed onboard and a model fit is made to the remaining data. The quality of the model fit can then be inspected visually.

[95] A further test can more directly determine how strongly any non-geophysical effects are contaminating the ULF electric field measurement. The short EFI boom is more strongly affected by asymmetric illumination and wake electric fields due to the voltage probes' closer proximity to the spacecraft. A comparison between the electric fields measured by the short and long booms can be used to determine the quality of the electric field measurement; if the wave electric fields measured by the short and long boom are very similar in amplitude and phase, it is less likely (although technically still possible) that spurious electric fields are significantly affecting the measurement of geophysical ULF electric fields.

[96] If only slow survey data are available, it still may be possible to check for contamination by comparing the EFI electric field with the electric field measured by ESA and FGM using the MHD approximation

$$\vec{E} = -\vec{v} \times \vec{B}$$

where E is the electric field, v is the either the electron or ion velocities measured by ESA, and B is the magnetic field measured by FGM. This comparison is only possible when ULF velocity perturbations are measured by ESA. This may not always be the case, as ESA itself is subject to several sources of contamination which cannot be removed during slow survey, and the ULF perturbations may be below ESA's detection threshold. Agreement between the ion and electron moment velocities is one indicator that the ESA instrument is effectively measuring ULF velocity perturbations. Major sources of contamination, such as penetrating radiation, affect the electron or ion flux measurements differently [*McFadden et al.*, 2008b]; agreement between the two measurements suggests that contamination does not significantly affect either measurement. Visual inspection of the energy flux spectrograms separately can also be used to check for contamination. If contamination is not significantly affecting the measurement of the velocity, the vxB electric field can be directly compared with the EFI electric field to check its validity.

[97] We inspected the quality of the electric field data for the three THEMIS probes in the magnetosphere. We found that both the phase and the amplitude of THA's measurement of the electric field were seriously contaminated for the entire interval described in the paper due to both boom shadowing and electrostatic wake effects. THD and THE data were useable for much of the interval. Figures and analysis showing the tests we conducted and the intervals with trustworthy data are shown in the auxiliary material.

[98] **Acknowledgments.** We acknowledge NASA THEMIS contract NAS5-02099; J. Bonnell and F. S. Mozer for use of the EFI data; and C. W. Carlson and J. P. McFadden for the use of the ESA data. We thank the NASA Space Science Data facility for use of solar wind data and geomagnetic activity indices. We thank the creators of the ONERA-DESP software library. The work done by Mark B. Moldwin was supported by NASA grant NNXAI626. The work done by Karl-Heinz Glassmeier was financially supported by the German Ministerium für Wirtschaft und Technologie and the Deutsches Zentrum für Luft- und Raumfahrt under grant 50OC1001.

[99] Robert Lysak thanks the reviewers for their assistance in evaluating this paper.

References

Agapitov, O., et al. (2009), Surface waves and field line resonances: A THEMIS case study, *J. Geophys. Res.*, *114*, A00C27, doi:10.1029/2008JA013553. [Printed *115*(A1), 2010.]

Allan, W., and D. R. McDiarmid (1993), Frequency ratios and resonance positions for magnetospheric cavity/waveguide modes, *Ann. Geophys.*, *11*, 916–924.

Allan, W., E. M. Poulter, and S. P. White (1986a), Hydromagnetic wave coupling in the magnetosphere–plasmapause effects on impulse-excited resonances, *Planet. Space Sci.*, *34*(12), 1189–1200, doi:10.1016/0032-0633(86)90056-5.

Allan, W., S. P. White, and E. M. Poulter (1986b), Impulse-excited hydromagnetic cavity and field-line resonances in the magnetosphere, *Planet. Space Sci.*, *34*(4), 371–385, doi:10.1016/0032-0633(86)90144-3.

Anderson, B. J., M. J. Engebretson, and L. J. Zanetti (1989), Distortion effects in spacecraft observations of MHD toroidal standing waves: Theory and observations, *J. Geophys. Res.*, *94*(A10), 13,425–13,445, doi:10.1029/JA094iA10p13425.

Auster, H. U., et al. (2008), The THEMIS fluxgate magnetometer, *Space Sci. Rev.*, *141*(1–4), 235–264, doi:10.1007/s11214-008-9365-9.

Bonnell, J. W., F. S. Mozer, G. T. Delory, A. J. Hull, R. E. Ergun, C. M. Cully, V. Angelopoulos, and P. R. Harvey (2008), The electric field instrument (EFI) for THEMIS, *Space Sci. Rev.*, *141*(1–4), 303–341, doi:10.1007/s11214-008-9469-2.

Carpenter, D. L., and R. R. Anderson (1992), An ISEE/Whistler model of equatorial electron density in the magnetosphere, *J. Geophys. Res.*, *97*(A2), 1097–1108, doi:10.1029/91JA01548.

Chandrasekhar, S. (1961), *Hydrodynamic and Hydromagnetic Stability*, Oxford Univ. Press, New York.

Chen, L., and A. Hasegawa (1974), A theory of long-period magnetic pulsations: 1. Steady state excitation of field line resonance, *J. Geophys. Res.*, *79*(7), 1024–1032, doi:10.1029/JA079i007p01024.

Cheng, C. Z., and C. S. Lin (1987), Eigenmode analysis of compressional waves in the magnetosphere, *Geophys. Res. Lett.*, *14*(8), 884–887, doi:10.1029/GL014i008p00884.

Claudepierre, S. G., M. Wiltberger, S. R. Elkington, W. Lotko, and M. K. Hudson (2009), Magnetospheric cavity modes driven by solar wind dynamic pressure fluctuations, *Geophys. Res. Lett.*, *36*, L13101, doi:10.1029/2009GL039045.

Darrouzet, F., et al. (2009), Plasmaspheric density structures and dynamics: Properties observed by the CLUSTER and IMAGE missions, *Space Sci. Rev.*, *145*(1–2), 55–106, doi:10.1007/s11214-008-9438-9.

Dungey, J. W. (1967), Hydromagnetic waves, in *Physics of Geomagnetic Phenomena*, edited by S. Matsushita and W. H. Campbell, pp. 913–934, Academic, San Diego.

Eriksson, P. T. I., L. G. Blomberg, S. Schaefer, and K.-H. Glassmeier (2006), On the excitation of ULF waves by solar wind pressure enhancements, *Ann. Geophys.*, *24*, 3161–3172, doi:10.5194/angeo-24-3161-2006.

Fairfield, D. H. (1971), Average and unusual locations of the Earth's magnetopause and bow shock, *J. Geophys. Res.*, *76*(28), 6700–6716, doi:10.1029/JA076i028p06700.

Fujita, S., K.-H. Glassmeier, and K. Kamide (1996), MHD waves generated by the Kelvin-Helmholtz instability in a nonuniform magnetosphere, *J. Geophys. Res.*, *101*(A12), 27,317–27,325, doi:10.1029/96JA02676.

Glassmeier, K. H. (1980), Magnetometer array observations of a giant pulsation event, *J. Geophys.*, *48*(3), 127–138.

Harrold, B. G., and J. C. Samson (1992), Standing ULF modes of the magnetosphere: A theory, *Geophys. Res. Lett.*, *19*(18), 1811–1814, doi:10.1029/92GL01802.

Hartinger, M., V. Angelopoulos, M. B. Moldwin, K.-H. Glassmeier, and Y. Nishimura (2011), Global energy transfer during a magnetospheric field line resonance, *Geophys. Res. Lett.*, *38*, L12101, doi:10.1029/2011GL047846.

Hasegawa, A. (1969), Drift mirror instability in the magnetosphere, *Phys. Fluids*, *12*(12), 2642–2650, doi:10.1063/1.1692407.

Junginger, H. (1985), Poynting vector as a diagnostic of hydromagnetic wave structure, *J. Geophys. Res.*, *90*, 4155–4163, doi:10.1029/JA090iA05p04155.

Kepko, L., and H. E. Spence (2003), Observations of discrete, global magnetospheric oscillations directly driven by solar wind density variations, *J. Geophys. Res.*, *108*(A6), 1257, doi:10.1029/2002JA009676.

Kepko, L., H. E. Spence, and H. J. Singer (2002), ULF waves in the solar wind as direct drivers of magnetospheric pulsations, *Geophys. Res. Lett.*, *29*(8), 1197, doi:10.1029/2001GL014405.

Kivelson, M. G., and D. J. Southwood (1985), Resonant ULF waves: A new interpretation, *Geophys. Res. Lett.*, *12*(1), 49–52, doi:10.1029/GL012i001p00049.

Kivelson, M. G., and D. J. Southwood (1986), Coupling of global magnetospheric MHD eigenmodes to field line resonances, *J. Geophys. Res.*, *91*(A4), 4345–4351, doi:10.1029/JA091iA04p04345.

Kivelson, M. G., M. Cao, R. L. McPherron, and R. J. Walker (1997), A possible signature of magnetic cavity mode oscillations in ISEE spacecraft observations, *J. Geomagn. Geoelectr.*, *49*(9), 1079–1098, doi:10.5636/jgg.49.1079.

Korotova, G. I., D. G. Sibeck, V. Kondratovich, V. Angelopoulos, and O. D. Constantinescu (2009), THEMIS observations of compressional pulsations in the dawn-side magnetosphere: A case study, *Ann. Geophys.*, *27*, 3725–3735, doi:10.5194/angeo-27-3725-2009.

Kouznetsov, I., and W. Lotko (1995), Radial energy transport by magnetospheric ULF waves: Effects of magnetic curvature and plasma pressure, *J. Geophys. Res.*, *100*(A5), 7599–7612, doi:10.1029/94JA02293.

Lee, D.-H., and K. Kim (1999), Compressional MHD waves in the magnetosphere: A new approach, *J. Geophys. Res.*, *104*(A6), 12,379–12,385, doi:10.1029/1999JA900053.

Lee, D. H., and R. L. Lysak (1989), Magnetospheric ULF wave coupling in the dipole model: The impulsive excitation, *J. Geophys. Res.*, *94*(A12), 17,097–17,103, doi:10.1029/JA094iA12p17097.

Lee, D.-H., and K. Takahashi (2006), MHD eigenmodes in the inner magnetosphere, in *Magnetospheric ULF Waves: Synthesis and New Directions*, *Geophys. Monogr. Ser.*, vol. 169, edited by K. Takahashi et al., pp. 73–89, AGU, Washington, D. C., doi:10.1029/169GM07.

Lin, N. G., L. J. Cahill, M. J. Engebretson, M. Sugiura, and R. L. Arnold (1986), Dayside pulsation events near the plasmapause, *Planet. Space Sci.*, *34*(2), 155–181, doi:10.1016/0032-0633(86)90112-1.

Mann, I., A. Wright, and P. Cally (1995), Coupling of magnetospheric cavity modes to field line resonances: A study of resonance widths, *J. Geophys. Res.*, *100*(A10), 19,441–19,456, doi:10.1029/95JA00820.

Mann, I. R., G. Chisham, and S. D. Bale (1998), Multisatellite and ground-based observations of a tailward propagating Pc5 magnetospheric waveguide mode, *J. Geophys. Res.*, *103*(A3), 4657–4669, doi:10.1029/97JA03175.

Mann, I., A. Wright, K. Mills, and V. Nakariakov (1999), Excitation of magnetospheric waveguide modes by magnetosheath flows, *J. Geophys. Res.*, *104*(A1), 333–353, doi:10.1029/1998JA900026.

McFadden, J. P., C. W. Carlson, D. Larson, M. Ludlam, R. Abiad, B. Elliot, P. Turin, M. Marckwordt, and V. Angelopoulos (2008a), The THEMIS ESA plasma instrument and in-flight calibration, *Space Sci. Rev.*, *141*(1–4), 277–302, doi:10.1007/s11214-008-9440-2.

McFadden, J. P., C. W. Carlson, D. Larson, J. Bonnell, F. Mozer, V. Angelopoulos, K.-H. Glassmeier, and U. Auster (2008b), THEMIS ESA first science results and performance issues, *Space Sci. Rev.*, *141*(1–4), 477–508, doi:10.1007/s11214-008-9433-1.

Mills, K. J., A. N. Wright, and I. R. Mann (1999), Kelvin-Helmholtz driven modes of the magnetosphere, *Phys. Plasmas*, *6*(10), 4070–4087, doi:10.1063/1.873669.

Mills, K. J., A. W. Longbottom, A. N. Wright, and M. S. Ruderman (2000), Kelvin-Helmholtz instability on the magnetospheric flanks: An absolute and convective instability approach, *J. Geophys. Res.*, *105*(A12), 27,685–27,699, doi:10.1029/1999JA000289.

Mozer, F. S. (1973), Analyses of techniques for measuring DC and AC electric fields in the magnetosphere, *Space Sci. Rev.*, *14*(2), 272–313, doi:10.1007/BF02432099.

Ni, B., Y. Shprits, M. Hartinger, V. Angelopoulos, X. Gu, and D. Larson (2011), Analysis of radiation belt energetic electron phase space density using THEMIS SST measurements: Cross-satellite calibration and a case study, *J. Geophys. Res.*, *116*, A03208, doi:10.1029/2010JA016104.

Plaschke, F., K.-H. Glassmeier, H. U. Auster, O. D. Constantinescu, W. Magnes, V. Angelopoulos, D. G. Sibeck, and J. P. McFadden (2009), Standing Alfvén waves at the magnetopause, *Geophys. Res. Lett.*, *36*, L02104, doi:10.1029/2008GL036411.

Rickard, G. J., and A. N. Wright (1994), Alfvén resonance excitation and fast wave propagation in magnetospheric waveguides, *J. Geophys. Res.*, *99*(A7), 13,455–13,464, doi:10.1029/94JA00674.

Rickard, G. J., and A. N. Wright (1995), ULF pulsations in a magnetospheric waveguide: Comparison of real and simulated satellite data, *J. Geophys. Res.*, *100*(A3), 3531–3537, doi:10.1029/94JA02935.

Samson, J. C., and G. Rostoker (1972), Latitude-dependent characteristics of high-latitude Pc 4 and Pc 5 micropulsations, *J. Geophys. Res.*, *77*(31), 6133–6144, doi:10.1029/JA077i031p06133.

Samson, J. C., B. G. Harrold, J. M. Ruohoniemi, R. A. Greenwald, and A. D. M. Walker (1992), Field line resonances associated with MHD waveguides in the magnetosphere, *Geophys. Res. Lett.*, *19*(5), 441–444, doi:10.1029/92GL00116.

Shue, J.-H., J. K. Chao, H. C. Fu, C. T. Russell, P. Song, K. K. Khurana, and H. J. Singer (1997), A new functional form to study the solar wind control of the magnetopause size and shape, *J. Geophys. Res.*, *102*(A5), 9497–9511, doi:10.1029/97JA00196.

Sibeck, D. G., and V. Angelopoulos (2008), THEMIS science objectives and mission phases, *Space Sci. Rev.*, *141*, 35–59, doi:10.1007/s11214-008-9393-5.

Southwood, D. J. (1974), Some features of field line resonances in the magnetosphere, *Planet. Space Sci.*, *22*(3), 483–491, doi:10.1016/0032-0633(74)90078-6.

Southwood, D., and M. Kivelson (1981), Charged particle behavior in low frequency geomagnetic pulsations: 1. Transverse waves, *J. Geophys. Res.*, *86*(A7), 5643–5655, doi:10.1029/JA086iA07p05643.

Southwood, D., and M. Kivelson (1993), Mirror instability: 1. Physical mechanism of linear instability, *J. Geophys. Res.*, *98*(A6), 9181–9187, doi:10.1029/92JA02837.

Southwood, D. J., J. W. Dungey, and R. J. Etherington (1969), Bounce resonant interaction between pulsations and trapped particles, *Planet. Space Sci.*, *17*(3), 349–361, doi:10.1016/0032-0633(69)90068-3.

Takahashi, K., C. Z. Cheng, R. W. McEntire, and L. M. Kistler (1990), Observation and theory of Pc5 waves with harmonically related transverse and compressional components, *J. Geophys. Res.*, *95*(A2), 977–989, doi:10.1029/JA095iA02p00977.

Takahashi, K., et al. (2010), Multipoint observation of fast mode waves trapped in the dayside plasmasphere, *J. Geophys. Res.*, *115*, A12247, doi:10.1029/2010JA015956.

Tsyganenko, N. A. (1989), A magnetospheric magnetic field model with a warped tail current sheet, *Planet. Space Sci.*, *37*(1), 5–20, doi:10.1016/0032-0633(89)90066-4.

Viall, N. M., L. Kepko, and H. E. Spence (2009), Relative occurrence rates and connection of discrete frequency oscillations in the solar wind density and dayside magnetosphere, *J. Geophys. Res.*, *114*, A01201, doi:10.1029/2008JA013334.

Walker, A., R. Greenwald, W. Stuart, and C. Green (1979), Stare auroral radar observations of Pc5 geomagnetic pulsations, *J. Geophys. Res.*, *84*(A7), 3373–3388, doi:10.1029/JA084iA07p03373.

Waters, C. L., K. Takahashi, D.-H. Lee, and B. J. Anderson (2002), Detection of ultralow-frequency cavity modes using spacecraft data, *J. Geophys. Res.*, *107*(A10), 1284, doi:10.1029/2001JA000224.

Wright, A. N. (1994), Dispersion and wave coupling in inhomogeneous MHD waveguides, *J. Geophys. Res.*, *99*(A1), 159–167, doi:10.1029/93JA02206.

Wright, A. N., and G. J. Rickard (1995), A numerical study of resonant absorption in a magnetohydrodynamic cavity driven by a broadband spectrum, *Astrophys. J.*, *444*, 458–470, doi:10.1086/175620.

Yang, B., Q. G. Zong, Y. F. Wang, S. Y. Fu, P. Song, H. S. Fu, A. Korth, T. Tian, and H. Reme (2010), Cluster observations of simultaneous resonant interactions of ULF waves with energetic electrons and thermal ion species in the inner magnetosphere, *J. Geophys. Res.*, *115*, A02214, doi:10.1029/2009JA014542.

Zhu, X., and M. Kivelson (1989), Global mode ULF pulsations in a magnetosphere with a nonmonotonic Alfvén velocity profile, *J. Geophys. Res.*, *94*(A2), 1479–1485, doi:10.1029/JA094iA02p01479.

Zhu, X., and M. G. Kivelson (1991), Compressional ULF waves in the outer magnetosphere: 1. Statistical study, *J. Geophys. Res.*, *96*(A11), 19,451–19,467, doi:10.1029/91JA01860.

Zhu, X., and M. Kivelson (1994), Compressional ULF waves in the outer magnetosphere: 2. A case study of Pc5 type wave activity, *J. Geophys. Res.*, *99*(A1), 241–252, doi:10.1029/93JA02106.